frontiers in Materials

REVIEW
published: 03 January 2022
doi: 10.3389/fmats.2021.792359

Mechanical Properties and Deformation Mechanisms of Heterostructured High-Entropy and Medium-Entropy Alloys: A Review

Wei Jiang[1], *Yuntian Zhu*[1,2] *and Yonghao Zhao*[1]*

[1]Nano and Heterogeneous Materials Center, School of Materials Science and Engineering, Nanjing University of Science and Technology, Nanjing, China, [2]Department of Materials Science and Engineering, City University of Hong Kong, Hong Kong, China

Recently, heterostructured (HS) materials, consisting of hard and soft zones with dramatically different strengths, have been developed and received extensive attention because they have been reported to exhibit superior mechanical properties over those predicted by the rule of mixtures. Due to the accumulation of geometrically necessary dislocations during plastic deformation, a back stress is developed in the soft zones to increase the yield strength of HS materials, which also induce forward stress in the hard zones, and a global hetero-deformation induced (HDI) hardening to retain ductility. High-entropy alloys (HEAs) and medium-entropy alloys (MEAs) or multicomponent alloys usually contain three or more principal elements in near-equal atomic ratios and have been widely studied in the world. This review paper first introduces concepts of HS materials and HEAs/MEAs, respectively, and then reviewed emphatically the mechanical properties and deformation mechanisms of HS HEAs/MEAs. Finally, we discuss the prospect for industrial applications of the HS HEAs and MEAs.

Keywords: high-entropy alloy, heterostructured material, microstructure, mechanical property, strength, ductility

OPEN ACCESS

Edited by:
John L. Provis,
The University of Sheffield,
United Kingdom

Reviewed by:
Zhiming Li,
Central South University, China
Bo Song,
Southwest University, China

***Correspondence:**
Yonghao Zhao
yhzhao@njust.edu.cn

Specialty section:
This article was submitted to Structural Materials, a section of the journal Frontiers in Materials

Received: *10 October 2021*
Accepted: *12 November 2021*
Published: *03 January 2022*

Citation:
Jiang W, Zhu Y and Zhao Y (2022) Mechanical Properties and Deformation Mechanisms of Heterostructured High-Entropy and Medium-Entropy Alloys: A Review. Front. Mater. 8:792359. doi: 10.3389/fmats.2021.792359

INTRODUCTION

Heterostructured Materials

Metallic materials with outstanding mechanical properties, especially high strength and ductility, are widely used in many engineering fields such as transportation, spacecraft, and industrial manufacture (Bouaziz et al., 2013; He et al., 2017; Zhao and Jiang, 2018). For example, super strong metallic materials can significantly reduce the weight of transport vehicles, thus improving their energy efficiency (Zhao and Jiang, 2018). Therefore, the development of metallic materials with high strength and ductility is an unremitting research subject for material scientists (Gao et al., 2020). Nowadays, the challenge for the industrial application of metallic materials is that the strength of most metallic materials is limited and needs to be further improved to meet the industrial requirements. Considering the internal mechanism that affects the strength and ductility of metallic materials, the strength of metallic materials depends on the hindrance of dislocation motion, while the ductility depends on the ability of dislocation activity, such as dislocation generation, accumulation, and movement (Hughes et al., 2003; Meyers and Chawla, 2008). Therefore, one of the traditional strengthening strategies for high-strength materials is to produce nanostructured materials by grain refinement through severe plastic deformation, such as equal-channel angular pressing (ECAP) and high-pressure torsion (HPT) (Cao et al., 2018).

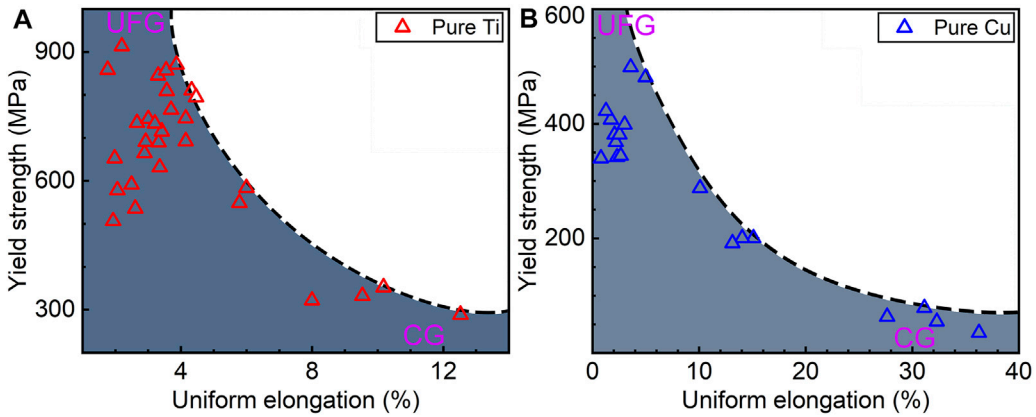

FIGURE 1 | Traditional strength–ductility trade-off relationship in pure **(A)** Ti and **(B)** Cu (Wang et al., 2002; Ritchie, 2011; Wu et al., 2015; Shahmir et al., 2016).

According to the empirical Hall–Petch relationship and classic Taylor hardening model, the strength of metallic materials monotonically increases with reducing grain size and increasing dislocation density (Taylor, 1934; Hansen, 2004). The introduction of substantial grain boundaries and high density of dislocations is a powerful approach for blocking dislocation movement and thus significantly enhances the strength of metallic materials (He et al., 2017; Jiang et al., 2021a). Moreover, the introduction of precipitates and solute atoms to induce precipitation hardening and solid solution strengthening are also effective means of strengthening (Zhao et al., 2004; Li et al., 2015; Jiang et al., 2021a).

Unfortunately, these traditional methods of introducing obstacles, e.g., grain boundaries, dislocations, precipitation, and solute atoms, to improve strength inevitably limit the multiplication and accumulation of dislocations. According to the Hart's theory (Hart, 1967) and the Considère criterion (Wei et al., 2004), higher dislocation storage capacity associated with dislocation multiplication and accumulation means higher strain hardening, which can help delay the onset of necking during plastic deformation and prolong ductility. Consequently, the enhancement of strength through the traditional strengthening mechanisms always leads to a degradation of ductility, which is referred to as the strength-ductility trade-off, as shown in **Figure 1** (Wang et al., 2002; Ritchie, 2011; Wu et al., 2015; Shahmir et al., 2016). Actually, the strength-ductility trade-off has always been a problem in the materials science community, because good ductility is simultaneously required for high-strength materials to prevent catastrophic failure during service (Wang and Ma, 2004; Ma and Zhu, 2017). Over the centuries, engineers have been forced to choose either strength or ductile of metallic materials, not both as desired (Zhu and Li, 2010).

Previous efforts to resolve this trade-off problem have been focused on boundary engineering such as coherent twin boundaries (Lu et al., 2004; Lu K. et al., 2009; Gutierrez-Urrutia and Raabe, 2011) and phase boundaries (Byun et al., 2004); the associated strengthening mechanisms are known as twinning-induced plasticity (TWIP) effect (Gutierrez-Urrutia and Raabe, 2011) and transformation-induced plasticity

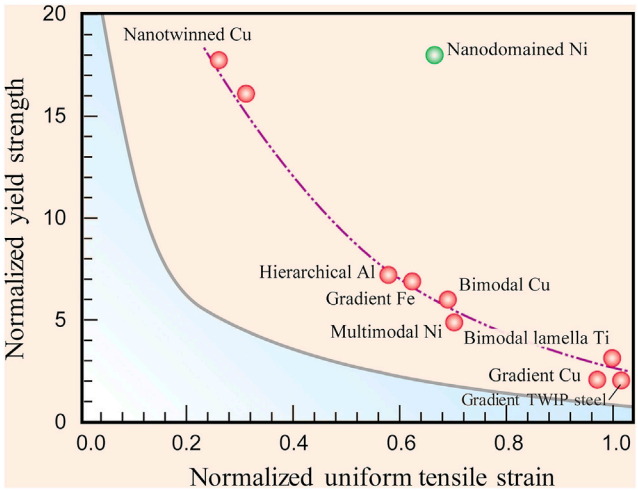

FIGURE 2 | Normalized yield strength versus normalized uniform tensile strain of metallic materials with homogeneous (banana-shaped shaded regions) and heterogeneous (solid circle) microstructures. Image adopted from Ref. Ma and Zhu (2017). with permission from Elsevier.

(TRIP) effect (Byun et al., 2004), respectively. TWIP and TRIP effects generate additional boundaries *in-situ* for dislocation storage and significantly reduce the effective grain size, resulting in secondary strain hardening (Byun et al., 2004; Gutierrez-Urrutia and Raabe, 2011, 2012; Zhu et al., 2012; Su et al., 2019) and enhanced ductility. Moreover, the preexisting twin boundaries can act as both obstacles to dislocation movement and pathways to dislocation slip and cross-slip, simultaneously enhancing the strength and ductility (Ming et al., 2019). However, there are still shortcomings: 1) their strength may reach a limit with reducing boundary spacing to nanometers (Lu L. et al., 2009; Li et al., 2010); 2) both the TWIP and TRIP effects are confined in materials with low stacking-fault energy (SFE) (Grässel et al., 2000; An et al., 2012); and 3) the yield strength is low, and a further increase in yield strength will still lead to a degradation of ductility (Bouaziz et al., 2011).

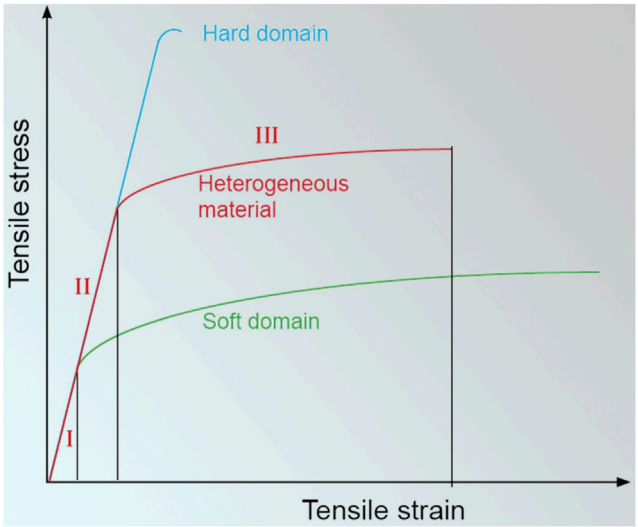

FIGURE 3 | The plastic deformation process of heterogeneous materials during tension. Image adopted from Ref. Wu and Zhu (2017) with permission from Taylor and Francis.

More recently, a novel concept of heterostructured (HS) materials has attracted increasing attention due to their superior strength-ductility combination (Zhu et al., 2020), as shown in **Figure 2**. After years of development, there are several types of HS materials, including bimodal grain structures (Wang et al., 2002; Han et al., 2005; Zhao et al., 2008), heterogeneous lamella structures (HLSs) (Wu et al., 2015; Li J. et al., 2019), gradient grain structures (Wu X. et al., 2014; Lu, 2014; Wei et al., 2014; Qin et al., 2019), laminate structures (Qin et al., 2019), dual-phase structures (Li et al., 2016), harmonic structures (Sawangrat et al., 2014), and metal matrix composites (Choudhuri et al., 2018; Liu et al., 2018). What they have in common is that all these HS materials consist of very diverse microstructures: the mixture of hard and soft zones with dramatically different strengths (Wu and Zhu, 2017). The strength difference between the hard and soft zones can be achieved by adjusting the crystal structures (Zhao et al., 2017), defect concentration (Yang M. et al., 2018; Ming et al., 2019), and just the grain size ranging from nanometers to millimeters (Wang et al., 2002). For example, a simple thermomechanical treatment of Cu skillfully avoids the traditional strength–ductility paradox through the bimodal grain structures, in which a small amount of micron-size grains randomly distribute in nanocrystalline (NC) and ultrafine grain (UFG) matrices (Wang et al., 2002).

The key concept for HS materials to increase strength while retaining ductility is to enhance the strain hardening ability and thus in turn delay plastic instability. As shown in **Figure 3**, HS materials experience a unique deformation process during tension, compared to homogeneous materials. Once loaded, both the hard and soft zones start elastic deformation first (Wu and Zhu, 2017). After the simultaneous elastic deformation stage, the soft zones begin plastic deformation, while the hard zones are still in elastic status. Constraints resulting from the hard zones will be imposed on the soft zones to inhibit its free plastic deformation. Consequently, geometrically necessary dislocations (GNDs) will be generated and pile up against zone interfaces due to mechanical incompatibility of hard and soft zones. The induced GNDs can produce long-range internal stress, i.e., back stress, in soft zones to offset the applied shear stress, making them appear stronger to withstand higher shear stress (Wu and Zhu, 2017; Zhu and Wu, 2019). Meanwhile, the stress concentration caused by dislocation piling up at zone interfaces induces forward stress in hard zones to make hard zones appear weaker (Zhu and Wu, 2019). As evidenced by the increasing works in recent years, the hetero-deformation-induced (HDI) hardening effect (Zhu and Wu, 2019), induced by the interaction between back stresses and forward stresses, exert extra strain hardening in HS materials and thus enhanced the yield strength and ductility (Zhu and Wu, 2019; Liu et al., 2020). With the flow stress further increasing, the hard zones start yielding to accommodate the stress concentration (Zhu and Wu, 2019). Finally, both the hard and soft zones are deforming plastically, while the soft zones bear higher plastic strain, leading to a strain partitioning. However, the continuity of zone boundaries requires the same plastic strain for adjacent soft and hard zones. Thus, strain gradient is necessary near the zone interface to accommodate the strain partitioning (Zhu and Wu, 2019). There is clear evidence that rapid accumulation of GNDs in the hetero-zone boundary-affected regions (HBARs) (Wu and Zhu, 2021) will result in a significant HDI effect at low strain (>4.5%), while dislocation hardening dominates at higher strain levels (Fang et al., 2020).

There is no doubt that the HS materials have microstructural requirements for the optimum mechanical properties, such as volume fraction of soft zones, interface spacing, and distribution of hard zones (Ma et al., 2016; Huang et al., 2018; Liu et al., 2020). For instance, thinner interface spacing results in a synergetic improvement of strength and ductility in copper/bronze laminates (Ma et al., 2016). In the vicinity of zone boundaries, the accumulation of GNDs results in a (HBAR) of a few micrometers. The optimum spacing is that the adjacent HBARs begin to overlap to maximize the hardening capacity, after which the strength–ductility trade-off occurred (Huang et al., 2018). Likewise, the volume fractions of the gradient structure have a significant influence on the strength and ductility of gradient structural pure copper (Yang et al., 2015). The optimum gradient structure volume fraction of 0.08–0.1 produces an excellent strength–ductility combination (Yang et al., 2015). Moreover, the strength–ductility combination in HS materials can be optimized by adjusting the volume and density of boundaries between the hard and soft zones to maximize the strain/stress partitioning and strain gradient between the zones (Ma and Zhu, 2017; Wu and Zhu, 2017). For guidance of material design, Zhu et al. have made numerous efforts to systematically study the effectiveness of various HS structural materials (Wu and Zhu, 2017). With regard to the gradient structures, the dynamic migration of interfaces from the coarse-grained core to the nanograined layer makes the successive deformation over the sample and suppresses strain localization (Lu, 2014). However, the limited interface density of

gradient structures weakens the density of accumulated dislocation and thus their capability of back-stress work hardening (Wu X. et al., 2014; Lu, 2014). For bimodal structures (Wang et al., 2002; Han et al., 2005; Zhao et al., 2008), the problem that still exists is that the limited interface density cannot effectively maximize the HDI stress strengthening potential. For dual-phase steels with hard zones embedded in the soft matrix, the continuous soft matrix induces high ductility but relatively low yield strength (Calcagnotto et al., 2011; Li et al., 2016). For harmonic structures with soft zones surrounded by hard zones, strength can be further improved by tuning the interface spacing and volume fraction of hard zones (Sawangrat et al., 2014). In contrast, the heterogeneous lamella structures (HLSs) present the best strength–ductility combination (Wu et al., 2015). By asymmetric rolling and partial recrystallization, HLS Ti featured with soft lamellae zones embedded in the hard lamella matrix was architected (Wu et al., 2015). The high constraint of the soft zones by the hard matrix renders high strength, and the strong strain partitioning also renders extraordinary strain hardening and consequent increased ductility (Wu et al., 2015).

High Entropy Alloy

While alloys of dilute solid solutions are still being researched, there is a continuous surge worldwide in developing alloys of concentrated solid solutions—medium-entropy alloys (MEAs) and high-entropy alloys (HEAs) (Zhang et al., 2014; Gludovatz et al., 2016; Ding et al., 2019). Different from traditional dilute solid solution alloys with only one principal element and some other elements in minor quantity, the MEAs/HEAs are nominally equiatomic or near-equimolar multicomponent alloys typically with three or more principal elements. This concept, first pointed out by Yeh et al. (Yeh et al., 2004) and Cantor et al. (Cantor et al., 2004), results in a paradigm shift in the alloy design concept toward the unexplored center region of the phase diagram and broadens the field of scope on alloy design (Miracle and Senkov, 2017; Sathiyamoorthi and Kim, 2020; Jiang et al., 2021b). MEAs are composed of three or more principal elements with near-equal atomic percentages (Gludovatz et al., 2016), and their configurational entropies are in the range of 1–1.5R (R = 8.314 mol−1·K−1). HEAs are comprised of five or more principal elements with near-equal atomic percentages (Zhang et al., 2014), and their configurational entropies are larger than 1.5R (Miracle et al., 2014). Due to the high mixing entropy associated with a disordered solution of several elements, both MEAs and HEAs can form stable single-phase solid solutions, in which atoms with different sizes are homogeneously distributed in the ideal situation. However, enthalpic interactions unavoidably change the local chemical order (LCO) in MEAs and HEAs, leading to short-range ordering (SRO) and/or incipient concentration waves. Notwithstanding the uncertainty of LCO, a mixture of atoms of diverse sizes results in severe lattice distortion, presenting frequent short-range resistance to dislocation slip, in this manner to maximize the solid solution strengthening effect in MEAs and HEAs (Yeh et al., 2007; Tsai et al., 2013; Li Q.-J. et al., 2019; Jiang et al., 2021c). Thus, the MEAs/HEAs exhibit remarkable properties and spark a lot of research interests among materials scientists.

After years of research, there are four unique core effects summarized in HEAs, which are relatively unusual in conventional alloys: high entropy effect, sluggish diffusion effect, lattice distortion effect, and cocktail effect (Tsai et al., 2013; Tsai and Yeh, 2014; Song et al., 2017; Li et al., 2021). These effects are closely related to the phase stability, microstructures, and mechanical properties of MEAs/HEAs. Nevertheless, the high entropy effect is still debatable. In some research, the high mixing entropy was confirmed that can stabilize MEA/HEA solution phases rather than intermetallic and complex phases (Yeh et al., 2004; Tsai and Yeh, 2014). Works on CoCrFeNi HEA argue the absence of long-range ordering, indicating the formation of really disordered solid solutions (Lucas et al., 2012). However, both first-principle density functional theory (DFT)-based simulations and direct experimental observation also verify the presence of LCO in MEAs/HEAs (Ding et al., 2018; Li Q.-J. et al., 2019; Chen et al., 2021).

Hitherto, it has been broadly demonstrated that both MEAs and HEAs have extraordinary mechanical properties over a wide temperature range from elevated to cryogenic temperatures (Jo et al., 2017; Yang M. et al., 2019; Gao et al., 2019; Jiang et al., 2021c). For instance, almost all the traditional high-temperature alloys tend to lose both strength and ductility at high temperatures, while equiatomic NbMoTaW and VNbMoTaW refractory HEAs sustain high strength at elevated temperatures more than 1,000°C (Senkov et al., 2011). At room and cryogenic temperatures, researchers attempt to introduce deformation substructures of stacking faults, deformation twins, and hexagonal close-packed (HCP) phase into MEAs/HEAs by tailoring the SFE (Zaddach et al., 2013). As evidenced by first-principle electronic structure calculations, the SFEs of MEAs/HEAs can be tuned by tailoring the atomic proportions of individual components. For example, the SFE of CrMnFeCoNi HEA is determined as approximately 25.5–27.3 mJm^{-2}, and that of $Cr_{26}Mn_{20}Fe_{20}Co_{20}Ni_{14}$ HEA is as low as 3.5 mJm^{-2} (Zaddach et al., 2013). These induced deformation substructures contribute to improve the strain hardening ability and leads to high tensile strength and ductility. As exemplified, Li et al. designed a metastable $Fe_{50}Mn_{30}Co_{10}Cr_{10}$ HEA to induce interface hardening and dynamic transformation induced hardening effects and consequently overcome the traditional strength–ductility trade-off (Li et al., 2016). Moreover, the prototypical Cantor alloy (CoCrFeMnNi) and its variants and subsets such as $Cr_{26}Mn_{20}Fe_{20}Co_{20}Ni_{14}$ HEA, CoCrFeNi HEA, and CoCrNi MEA are proven to possess remarkable cryogenic properties such as enhanced strength and ductility and superior fracture toughness, which are ascribed to their low SFEs and high propensity for twinning and phase transformation (Zaddach et al., 2013; Gludovatz et al., 2014; Gludovatz et al., 2016). More recently, LCO is confirmed to have significant influence on the SFE, which results in the increase of the SFE with the increase of the LCO (Ding et al., 2018). Furthermore, LCO affects the critical stress for dislocation slip and dislocation storage capacity in the bulk material, thus in turn affecting strain

hardening in single phase MEAs/HEAs (Jiang et al., 2021c). The dislocation slip in MEAs/HEAs has to continuously overcome the activation barriers created by LCO. In turn, MEAs/HEAs with LCO may exhibit higher strength.

Unfortunately, the yield strength of MEAs/HEAs is relatively low, especially for those with single-phase face-centered cubic (FCC) structures, which will greatly limit their industrial application prospects. Traditional methods to improve yield strength, such as solid solution strengthening (He et al., 2020), precipitation strengthening (Ming et al., 2017), and grain boundary strengthening (Sathiyamoorthi et al., 2019b), inevitably cause a degradation of ductility. The simple MEAs/HEAs are not exempted from the dilemma of the strength–ductility trade-off. Therefore, based on the novel alloy design concept with multi-principal elements, it is anticipated to achieve superior mechanical properties by further tuning the microstructures of HEAs/MEAs to fabricate HS structures. This review paper introduces the concept of HS MEAs/HEAs and then emphatically overviews the mechanical properties and deformation mechanisms of HS MEAs/HEAs. Finally, we discuss the prospects and industrial applications of the HS MEAs/HEAs.

HS HEAS

Heterogeneous Gradient Structure

A typical gradient structure is featured by a microstructural gradient at a macroscopic scale, which shows gradually increased grain size, increased substructure size, and reduced defect density from the surface layer to the interior layer (Wu X. L. et al., 2014; Yang et al., 2016; Bian et al., 2017; Pan et al., 2021). Due to the existing grain size gradient and/or the defect density gradient, the gradient structures possess prominent mechanical incompatibility, thus in turn leading to a macroscopic strain gradient and complex stress state, which needs to be accommodated by accumulated GNDs. The gradient structural materials usually show superior strength–ductility synergy, which are ascribed to either mechanically driven grain growth of the unstable nanostructured surface layer (Fang et al., 2011) or extra strain hardening caused by the presence of the strain gradient combined with the stress state change for the mechanically stable gradient structure (Wu X. et al., 2014; Wu X. L. et al., 2014; Bian et al., 2017). The intrinsic synergetic strengthening effect induced by the gradient structure is even much higher than the sum of the strength of individual layers, as calculated by the rule of mixtures (Wu X. L. et al., 2014).

The common methods for producing gradient materials include surface mechanical grinding treatment (SMGT) (Li et al., 2008), surface mechanical rolling treatment (SMRT) (Chen et al., 2020), surface mechanical attrition treatment (SMAT) (Yang et al., 2016), and rotationally accelerated shot peening (RASP) (Hasan et al., 2019; Liang et al., 2020). However, these surface treatment techniques produce only thin nanostructured surface layers with a depth of a few hundred micrometers (~200 μm) along the thickness direction of materials. In contrast, torsion, especially the HPT process, can produce larger-scale gradient structures along the diameter of the samples (Cao et al., 2011; Cao et al., 2014).

RASP was used to prepare gradient structural CoCrFeNiMn HEA (Hasan et al., 2019). Along the thickness direction, there exist gradient microstructures (**Figure 4**), such as gradients in twin and dislocation densities, and hierarchical nanotwin, which contribute to the strain hardening capability and mechanical properties (Hasan et al., 2019). Compared to the coarse grain (CG), the CoCrFeNiMn HEA with gradient structures (RASP1) shows enhanced strength (418 MPa) and ductility (45%) (**Figure 4**) (Hasan et al., 2019). However, an appropriate gradient structure profile is essential for the effective improvement of mechanical properties. Simultaneously enhanced strength and ductility can be realized in a gradient structure with an undeformed core sandwiched between two thin deformed surface layers (RASP1), while the fully deformed gradient structure profile (RASP3) will double the yield strength but sacrifice ductility (Hasan et al., 2019). This is due to the higher strain gradient in the gradient samples with the thin gradient structure profile, thus in turn promoting the generation and accumulation of GNDs to enhance the yield strength and strain hardening.

Gradient structures produced by SMRT are closely related to the processing passes, in which the depth of the surface gradient layer increases with increasing SMRT passes. For the $(Fe_{40}Mn_{40}Co_{10}Cr_{10})_{96.7}C_{3.3}$ HEA with a gradient structure, enhanced strength (from 429 to 765 MPa) together with considerable ductility (20.5%) is achieved, due to the high HDI hardening (Chen et al., 2020). The gradient structure containing dislocations and twins produces multiaxial stress state and strain gradient under tensile deformation, which contributes to the accumulation of GNDs, leading to the improvement of strength higher than the prediction of the rule of mixture.

Cyclic dynamic torsion (CDT) processing was used to obtain a gradient microstructural $Al_{0.1}$CoCrFeNi HEA (Chen et al., 2019a; Chen et al., 2019b). Along the radial direction, grain size gradually decreases from CG (~130 μm) at the center to fine grain (FG, ~8 μm) at the surface layer, as shown in **Figure 5**. Moreover, numerous deformation structures, such as deformation twins, dislocations, and microbands, form due to the torsional strain. The gradient structure results in a gradient distribution of hardness, which decreases from 3.4 GPa in surface layers to 2.6 GPa at the center (Chen et al., 2019a). A combination of high yield strength (850 MPa) and ductility (19%) indicates the important role of gradient microstructures (Chen et al., 2019b). More recently, Pan et al. designed a novel gradient nanoscaled dislocation–cell structures in $Al_{0.1}$CoCrFeNi HEA, which lead to enhanced strength (539 MPa) and little sacrificed ductility (42.6%) (Pan et al., 2021). Numerous low-angle dislocation cells provide nucleation sites for the formation of stacking faults and deformation twins, thereby contributing to extra strengthening, work hardening, and ductility (Pan et al., 2021).

Asymmetric rolling (ASR) followed by annealing is a novel strategy for producing CoCrFeMnNi HEA with gradient microstructures (Han et al., 2018). Different from the homogeneous structures achieved by symmetric rolling and

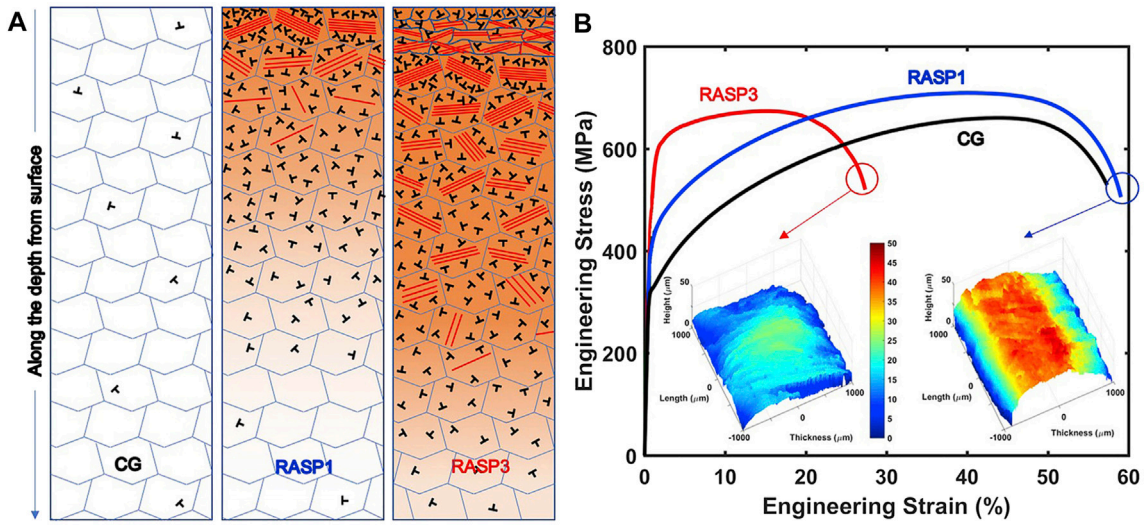

FIGURE 4 | (A) Gradient microstructures of CG, RASP1, and RASP3 samples along depths from the surface. **(B)** Engineering stress–strain curves for CG, RASP1, and RASP3 samples. Insets are the 3D surface topography for RASP1 and RASP3 after tensile deformation. Image adopted from Ref. Hasan et al. (2019) with permission from Elsevier.

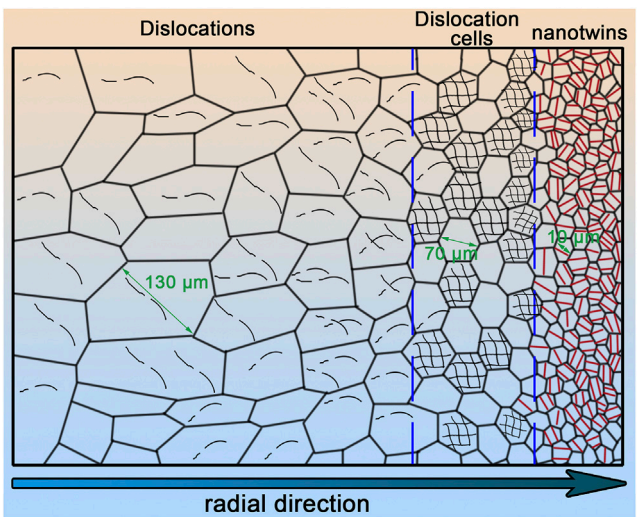

FIGURE 5 | A schematic diagram of the gradient microstructural $Al_{0.1}$CoCrFeNi HEA after DT processing, showing coarse grain area, intermediate area, and the fine grain area along the radial direction (Chen et al., 2019b; Mao et al., 2021).

annealing treatment, ASR and subsequent annealing processing produce a gradient structure. The surface layers contain UFGs (~500 nm), while the center consists of FGs (~2 μm) (Han et al., 2018). The combined effects of fine-grain strengthening and HDI hardening induced by the gradient microstructure give rise to a superior combination of strength (930 MPa) and ductility (42%).

During the tensile deformation of gradient structures, elastic–plastic deformation occurs immediately after the initial elastic deformation between the center CG regions and the gradient surface layer, thus in turn resulting in an elastic–plastic interface. As the deformation continues, the grains in the inner gradient layer gradually reach the yielding state and begin to deform plastically, leading to the dynamic movement of the elastic–plastic interface toward the surface. Due to the mechanical incompatibility between the center CG regions and the gradient surface layer, they significantly constrain each other during tensile deformation (Yang et al., 2015; Li et al., 2017). The CG core is subjected to tensile stresses laterally, while the gradient surface layer is subjected to compressive stresses along the gradient direction. These biaxial stress states can effectively activate more slip systems and improve the dislocation activities. Moreover, the mutual constraint between the central CG region and the gradient layer during the plastic deformation results in strain gradients near the interfaces to sustain the strain continuity, causing the generation and accumulation of GNDs at the interface. Some surface treatment processes, e.g., SMAT and SMRT, will also introduce the compressive stress, developing multiaxial stress states (Moering et al., 2016). The combined effect of the piling-up of GNDs and multiaxial stress states results in the superior strength–ductility combination in gradient structural materials (**Table 1**).

It has been substantiated that there exist optimal gradient thickness condition and microstructures within the gradient layer to optimize the strain hardening capacity and mechanical properties. Hasan et al. (Hasan et al., 2019) used different RASP parameters to produce a series of gradient structural CoCrFeNiMn HEAs with different gradient structural profiles. This accordingly results in different mechanical properties. Among the gradient structural CoCrFeNiMn HEAs, samples subjected to more severe deformation exhibit an obvious fine-grained layer, while those subjected to mild deformation only exhibit TBs, high-angle grain boundaries, and low-angle grain boundaries distributed along the gradient direction (Hasan et al.,

TABLE 1 | List of the processing steps (P), yield strength (YS), ultimate tensile strength (UTS), and uniform elongation (UE) of MEAs/HEAs reported with gradient structure. AN—annealing; EP-USR—electropulsing-assisted ultrasonic surface rolling; SP—shot peening.

Alloys	P	YS (MPa)	UTS (MPa)	UE (%)	References
CoCrFeMnNi	ASR, AN	700	930	42	Han et al. (2018)
$Al_{0.1}$CoCrFeNi	CDT	510	850	19	Chen et al. (2019b)
$Al_{0.1}$CoCrFeNi	CT	539	690	42	Pan et al. (2021)
$(Fe_{40}Mn_{40}Co_{10}Cr_{10})_{96.7}C_{3.3}$	SMRT	587	885	40.4	Chen et al. (2020)
$(Fe_{40}Mn_{40}Co_{10}Cr_{10})_{96.7}C_{3.3}$	SMRT	765	956	20.5	Chen et al. (2020)
CrCoFeNiMn	RASP	418	720	45	Hasan et al. (2019)
CrCoFeNiMn	RASP	610	680	15	Hasan et al. (2019)
CoCrFeMnNi	EP-USR	750	802	21.9	Xie et al. (2020a)
$CoCrFeNiMo_{0.15}$	Torsion	724	904	27	Wu et al. (2017)
$FeCoCrNiMo_{0.15}$	SP	486	855	46.8	Guo et al. (2020)
CoCrNi	Torsion	760	880	31	Liu et al. (2021a)
CoCrNi	Torsion, AN	930	1,050	27	Liu et al. (2021b)

TABLE 2 | List of the heterogeneous structures (H) and mechanical properties of MEAs/HEAs reported with heterogeneous grain structure. "-" represents the compressive test.

Alloys	H	YS (MPa)	UTS (MPa)	UE (%)	References
$Co_{25}Ni_{25}Fe_{25}Al_{7.5}Cu_{17.5}$	NG + UFG	-1795	-1936	-10.6	Fu et al. (2016)
$Ti_{10}Fe_{30}Co_{30}Ni_{30}$	NG + CG	-1830	-2024	-18.7	Fu et al. (2018)
$Cr_{20}Fe_6Co_{34}Ni_{34}Mo_6$	FG + UFG	1,100	1,300	29	Ming et al. (2019)
$V_{10}Cr_{15}Mn_5Fe_{35}Co_{10}Ni_{25}$	FG + CG	761	936	28.3	Jo et al. (2017)
$Al_{0.1}$CoCrFeNi	UFG + FG + CG	711	928	30.3	Wu et al. (2019b)
$Al_{0.1}$CoCrFeNi	FG + CG	525	784	37	Wang et al. (2019)
CrMnFeCoNi	FG + UFG	625	855	50.7	Bae et al. (2017)
CoCrFeNiMn	UFG + CG	1,298	1,390	9.4	Xie et al. (2020b)
CoCrNi	NG + UFG + FG	1,150	1,320	22	Yang et al. (2018a)
CoCrNi	UFG + FG	797	1,360	19	Slone et al. (2019)
CoCrNi	FG + UFG	928	1,191	28	Sathiyamoorthi et al. (2019a)
CrCoNi	CG + NG	1,452	1,520	10	Schuh et al. (2019)
CoCrNi	UFG + FG	1,435	1,580	24	Sathiyamoorthi et al. (2019b)

2019). The former shows the dramatic improvement of yield strength but scarified ductility, while the latter shows the simultaneously enhanced strength and ductility (**Figure 4**). This is attributed to the optimal gradient structures of a sandwich structure with a CG core and a thin layer of gradient structure on each side of the surface, improving mechanical properties due to the hierarchical twin structures in the gradient structural layers and the prominent strain gradient induced during the subsequent tensile deformation (Hasan et al., 2019). Besides, the surface treatment processes and the geometry of the tensile samples will lead to the difference in stress state and thus in turn influence the mechanical properties of the materials with gradient structures (Moering et al., 2016). For example, the SMAT and RASP processes can produce rod and flat samples, respectively. For the former, the ductile core is fully confined by the hard-outer surface and subjected to complex stress states, while for the latter, the ductile core is not confined in the lateral surface and subjected to biaxial stress states (Hasan et al., 2019; Chen et al., 2020).

Heterogeneous Grain Structure

"Smaller is stronger" means that grain refinement from CG to nano-grain (NG) results in extreme improvement in strength for conventional materials. However, low ductility has always been a problem for NG materials. Scientists are always looking for materials that have both the strength of NG and the ductility of CG. Recently, a heterogeneous material with bimodal and/or multimodal grain structures is a novel material design strategy to unite the advantages of both CG materials and NG materials, which present high strain hardening rate and superior strength and ductility combination (Wang et al., 2002).

Inspired by this concept, many strategies are explored to produce bimodal structural materials (**Table 2**). Both bimodal $Fe_{30}Co_{30}Ni_{30}Ti_{10}$ MEA and $Fe_{25}Co_{25}Ni_{25}Al_{7.5}Cu_{17.5}$ HEA produced by mechanical alloying and following spark plasma sintering exhibit high compressive strength (>1.7 GPa) and enhanced plasticity, as compared to their CG counterparts (Fu et al., 2016; Fu et al., 2018). The combined effect of local temperature gradient in SPS processing and sluggish diffusion effect of MEAs/HEAs results in the inhomogeneous grain size, where the $Fe_{30}Co_{30}Ni_{30}Ti_{10}$ MEA consists of CGs (>1 μm) and NGs and the $Fe_{25}Co_{25}Ni_{25}Al_{7.5}Cu_{17.5}$ HEA is comprised of NGs and UFGs (>200 nm) (Olevsky and Froyen, 2009; Tsai et al., 2013). HPT followed by annealing processing successfully produces bimodal microstructures in CoCrNi MEA (Sathiyamoorthi et al., 2019b; Schuh et al., 2019). Annealing parameters such as temperature and time play an important role in the ratio of bimodal grains and thus in turn influence the

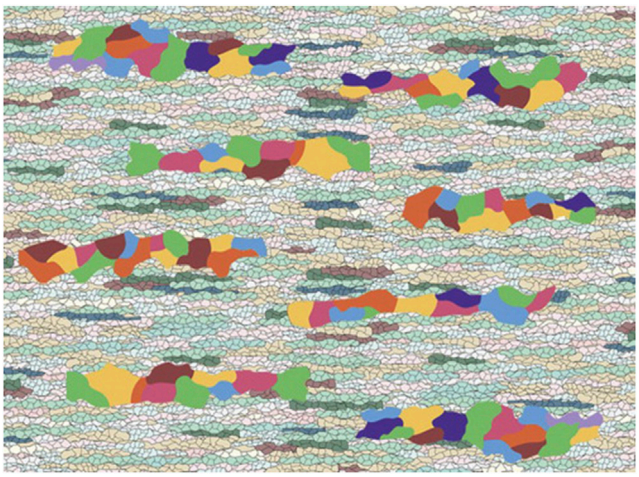

FIGURE 6 | Schematics of the lamella structure with elongated soft coarse-grained domains embedded in an ultrafine-grained matrix. Image adopted from Ref. Wu and Zhu (2017) with permission from Taylor and Francis.

mechanical properties. For the CoCrNi MEA annealed at 500°C/100 h, the mixture of NG and FG structures gains the ultra-high strength (1,500 MPa) and decent ductility (10%) combination (Schuh et al., 2019). By contrast, Sathiyamoorthi et al. (Sathiyamoorthi et al., 2019b) doubled the ductility (24%) of CoCrNi MEA with comparable strength (1,580 MPa) *via* HPT and followed annealing processing (600°C/1 h). Bimodal grain structures comprised of UFGs and FGs are responsible for the superior strength–ductility synergy. This observation indicates that the bimodal grain structure with UFGs and FGs seems to be better than that with NGs and FGs.

More strikingly, material design strategies for fabricating three-level heterogeneous grain structures, characterized by mixture of NGs, UFGs, and FGs, are successfully controlled (**Table 2**). Through partial recrystallization, Yang et al. (Yang M. et al., 2018) produced a HS CoCrNi MEA with a large span of grain size from NG to FG, imparting gigapascal yield strength (1,150 MPa) and high ductility (22%). Similarly, the $CoCrFeNiAl_{0.1}$ HEA with multiscale grains was produced by cold-rolling and intermediate temperature annealing, which is featured by three types of grains consisting of stretched grains (~20 μm), deformed grains (1–20 μm), and recrystallized grains (0.2–5 μm) (Wu S. W. et al., 2019). The thermomechanical treatments induced a difference in grain sizes, and dislocation density leads to a superior combination of yield strength (711 MPa) ductility (30.3%) (Wu S. W. et al., 2019).

According to the "smaller is stronger," NGs and/or UFGs in either bimodal or multimodal MEAs/HEAs serve as hard zones, while CGs serve as soft zones. Such HS materials present extra strain hardening ability, attributing to the generation and accumulation of GNDs to accommodate the strain gradient at zone interface (Wang et al., 2002). Moreover, partitioning of stress and strain comes into being at the zone interface, inducing a high stress concentration upon plastic deformation. Such stress concentration will achieve the critical resolved shear stress (CRSS) for twinning and generate twinned NGs, which in turn results in greater inhomogeneity (Yang M. et al., 2018). Significant HDI hardening effects together with the TWIP effects result in the superior strength–ductility synergy.

HLS

The HLS is featured by the soft micro-grained lamellae embedded in the hard UFG/NG lamella matrix (**Figure 6**). This material design strategies can also effectively unite the advantages of both CG materials and nanostructured materials to achieve excellent mechanical properties. Wu et al. (Wu et al., 2015) produced an HLS Ti, which presents an unprecedented property combination: as strong as UFG metals and as ductile as CG metals (Wu et al., 2015). HDI stress results in the unusual high strength, while HDI hardening and dislocation hardening lead to the high ductility (Wu et al., 2015).

For fabricating the HLSs, some approaches are typically employed, such as powder metallurgy with different size particles and asymmetrical rolling followed by annealing to obtain recrystallization with laminar distribution (Wu et al., 2015; Huang et al., 2017). Zhang et al. (Zhang et al., 2018; Zhang et al., 2019) successfully produced two kinds of MEAs with HLSs through thermomechanical processing (rolling and annealing). After cold rolling, numerous deformed structures, such as deformation bands, shear bands, and microbands, are formed, which depends on the original grain size (Zhang et al., 2019). After subsequent annealing, these deformed structures evolve into different annealing structures, forming HLSs. Partial recrystallization occurs to form recrystallized grains with sizes between 3 and 7 μm in the shear bands due to the high dislocation density (Zhang et al., 2019), while some UFGs with sizes less than 1 μm form in the large deformation bands (Zhang et al., 2019). The difference in the fraction of precipitates between the large deformation bands and shear bands has great influence on the behavior of recrystallization and grain growth. With increasing annealing time, the recrystallization and grain growth in large deformation bands occur, while these behaviors are much slower in shear bands due to the much more precipitate-induced Zener pinning effect (Zhang et al., 2018; Zhang et al., 2019). Thus, the rolling and subsequent annealing process results in the nonuniform grain size and the formation of the HLSs comprising of a UFG-FG lamella structure or FG-CG lamella structure (Zhang et al., 2019). The HS structure leads to a good combination of strength and ductility compared to simple FG and CG samples (Zhang et al., 2018).

The key advantage of materials with HLSs is the enhanced strain hardening ability (Wu et al., 2015; Wu and Zhu, 2017), which can prevent the early onset of necking (Hart, 1967). Due to the distribution of soft and hard lamella structures, corresponding to the CG and UFG grains, lots of GNDs are introduced to accommodate the strain gradients in order to avoid the formation of voids during the loading process. UFG lamellae with higher yield strength surround and constrain the soft CG lamellae, leading to the accumulation and block of dislocations in the CGs. Thus, yielding occurs in CG lamellae first due to the higher resolved shear stress from dislocation pile-

TABLE 3 | List of the heterogeneous structures and mechanical properties of MEAs/HEAs reported with HLSs.

Alloys	H	YS (MPa)	UTS (MPa)	UE (%)	References
FeNiCoAlTaB	FG + UFG	586	1,050	23	Zhang et al. (2019)
FeNiCoAlTaB	FG + CG	484	890	43	Zhang et al. (2019)
FeNiCoAlCrB	FG + CG	330	690	34	Zhang et al. (2018)
FeNiCoAlTaB	FG + CG	851	1,400	30	Zhang et al. (2020)
FeNiCoAlTaB	FG + CG	1,100	1700	10	Zhang et al. (2020)

TABLE 4 | A collection of reported HEAs with completely eutectic microstructure.

Alloys	Eutectic structure	YS (MPa)	UTS (MPa)	UE (%)	References
$AlCrFeNi_3$	(FeCrNi)-FCC + (AlNi)-B2	626	1,200	10.1	Dong et al. (2020)
$CrFeNi_{2.2}Al_{0.8}$	(FeCrNi)-FCC + (AlNi)-B2	479	956	12.7	Jin et al. (2019)
$Ni_{30}Co_{30}Cr_{10}Fe_{10}Al_{18}W_2$	(FeCoCrNi)-FCC + (AlNi)-B2	700	1,266	20.3	Wu et al. (2019a)
$Fe_{20}Co_{20}Ni_{41}Al_{19}$	(Fe, Co)-rich $L1_2$ + (AlNi)-B2	577	1,103	18.7	Jin et al. (2018b)
$Fe_{28.2}Ni_{18.8}Mn_{32.9}Al_{14.1}Cr_6$	(Fe, Mn, Ni)-FCC + (AlNi)-B2	599	868	19.5	Baker et al. (2016)
$Fe_{36}Ni_{18}Mn_{33}Al_{13}$	(Fe, Mn, Ni)-FCC + (AlNi)-B2	270	578	22.8	Wang et al. (2016)
$Al_{17}Co_{14.3}Cr_{14.3}Fe_{14.3}Ni_{40.1}$	$L1_2$ + B2	479	1,067	14	Jin et al. (2018a)
$Al_{17}Co_{28.6}Cr_{14.3}Fe_{14.3}Ni_{25.8}$	FCC + B2	476	1,001	14.8	Jin et al. (2018a)
$Al_{17}Co_{14.3}Cr_{14.3}Fe_{28.6}Ni_{25.8}$	FCC + B2	731	1,145	10.3	Jin et al. (2018a)

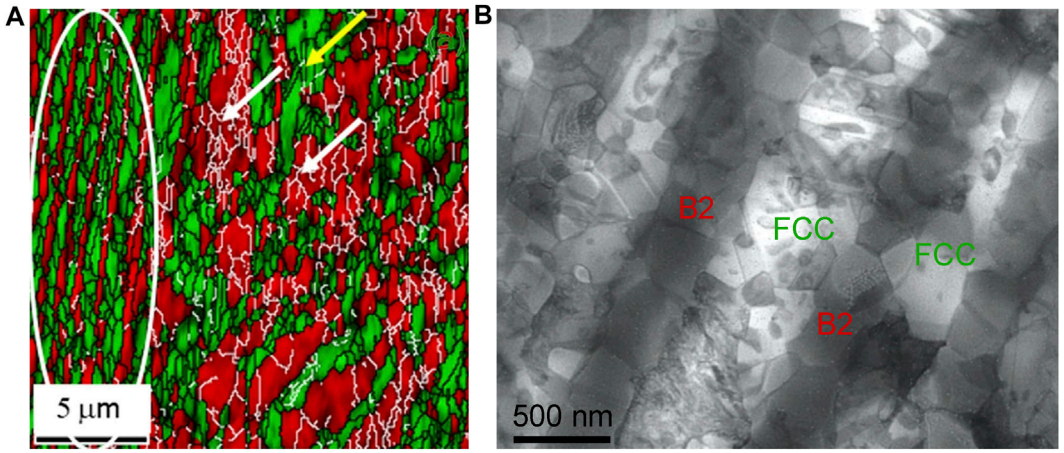

FIGURE 7 | Eutectic lamellate structures in $AlCoCrFeNi_{2.1}$ HEA by thermomechanical treatments. **(A)** Cryo-rolling and annealing (Bhattacharjee et al., 2018), **(B)** cold-rolling and annealing (Shi et al., 2019). Image adopted with permission under the terms of Creative Common License.

ups at the CG/UFG interface (Eshelby et al., 1951). Pile-ups of GNDs will also induce the long-range back stress, which resists the movement of dislocations in the CG lamellae and thus enhance strain hardening (Wu et al., 2015). With further increase in tensile load, the UFG lamellae begin plastic deformation, and hence the overall strength is enhanced by the HDI stress. The MEAs/HEAs with HLSs present remarkable mechanical properties, as shown in **Table 3**.

Heterogeneous Phase Structure

Eutectic structure

The approach of introducing two phases has been successfully used in MEAs/HEAs such as eutectic HEAs (Lu et al., 2014; Gao et al., 2017). Generally, the eutectic HEAs consist of alternate layers of soft FCC and hard B_2 phases (Baker et al., 2016; Wang et al., 2016; Jin et al., 2018b; a; Jin et al., 2019; Wu Q. et al., 2019; Dong et al., 2020), which possess a dramatic difference in strength and hardness. Like conventional dual-phase steel, the eutectic HEAs are typical HS materials that present a superior combination of strength and ductility, as shown in **Table 4**.

Among the numerous eutectic HEAs, $AlCoCrFeNi_{2.1}$ is the most widely investigated. Through different thermomechanical treatments, such as warm-rolling, cryo-rolling, cold-rolling, and subsequent annealing process, the heterogeneous microstructures of the $AlCoCrFeNi_{2.1}$ eutectic HEA can be further tuned to achieve superior mechanical properties, as shown in **Figure 7** (Bhattacharjee et al., 2018; Shukla et al., 2018; Reddy et al., 2019; Shi et al., 2019). Warm-rolled (750°C) $AlCoCrFeNi_{2.1}$ eutectic

TABLE 5 | List of the processing steps (P), eutectic structure (S) and mechanical properties of reported eutectic HEAs. AC–—as cast, WR—warm rolling, CR—cold rolling, CryoR—cryo rolling, AN—annealing, A—aging.

Alloys	P	S	YS (MPa)	UTS (MPa)	UE (%)	References
$AlCoCrFeNi_{2.1}$ eutectic HEA	AC	FCC + B2		1,100	18	Gao et al. (2017)
	WR		1,192	1,635	18	Reddy et al. (2019)
	50%CR, AN		1,110	1,340	10	Shukla et al. (2018)
	84%CR, AN		1,490	1,638	16	Shi et al. (2019)
	CryoR, AN		1,437	1,562	14	Bhattacharjee et al. (2018)
	70%CR, AN, A		1,009	1,476	19	Xiong et al. (2020)

HEA presents a heterogeneous microstructure characterized by the mixture of the retained lamellar region of B2 and FCC with B2 phases inside the FCC lamellar and non-lamellar regions consisting of disordered FCC, precipitated B2, and Cr-rich sigma phases (Reddy et al., 2019). The heterogeneous microstructures produced by cold-rolling and cryo-rolling and subsequent annealing are quite different. Through cold-rolling and following annealing, the $AlCoCrFeNi_{2.1}$ eutectic HEA consists of hard and soft lamellae with recrystallized grains and substantial B2 precipitates (Shukla et al., 2018; Shi et al., 2019). The cryo-rolling and subsequent annealing result in an HLS comprising of fine alternative FCC and B2 lamellar structures and coarse non-lamellar regions (Bhattacharjee et al., 2018). The fine FCC and B2 lamellae are filled with recrystallized UFGs (~200–250 nm) and low-angle grain boundaries, respectively, while the coarse non-lamellar regions are featured by ultrafine FCC (~200–250 nm), coarse recrystallized FCC grains, and coarse uncrystallized B2 phase (~2.5 μm) (Bhattacharjee et al., 2018). However, the Cr-rich sigma phases observed in the warm-rolled (750°C) $AlCoCrFeNi_{2.1}$ eutectic HEA were not observed in the HEA processed by cold-rolling and cryo-rolling.

Despite of the difference in thermomechanical treatments, all these remarkable HS $AlCoCrFeNi_{2.1}$ eutectic HEAs with high lamella density obtain an outstanding strength–ductility combination with gigapascal yield strength and ductility of over 15% (**Table 5**). This is attributed to the constraint effect originated from the lamellae. Upon plastic deformation, the hard B2 lamellae and the intergranular B2 precipitates provide rigid deformation constraint to FCC lamellae, resulting in generation and accumulation of GNDs at the lamellar interface and at the FCC-B2 interphase. This in turn makes the soft FCC lamellae stronger and improves the overall yield strength of $AlCoCrFeNi_{2.1}$ eutectic HEAs. Further plastic deformation results in the synergistic deformation of both hard and soft lamellae, with soft FCC lamellae bearing a higher strain, leading to the more substantial HDI hardening effect. Moreover, the aligned lamellar structure and ductile FCC matrix can delay crack propagation and coalescence, thereby delaying the onset of global necking (Shi et al., 2019; Shi et al., 2021).

Precipitation structure

As utilized in traditional materials, precipitations can be introduced in the grain interior to enhance the accumulation of dislocations when they intersect or bypass precipitations. This will result in strain hardening and consequently higher ductility. Moreover, the precipitations will impede the slip of dislocations and increase the stress required for dislocation movement. Thus, precipitation strengthening is an important strategy for improving the yield strength of MEAs/HEAs. This approach has been reported by several groups with the addition of Al, Cu, and Mo alloying elements to produce multiphase structures. Various kinds of precipitations, such as σ, μ, B2, BCC, and $L1_2$ phases, have been compounded in MEAs/HEAs to achieve superior mechanical properties (**Table 6**). It should be noted that, in order for this approach to be effective, the concentration of the alloying elements and the thermomechanical processing need to be optimized (Shahmir et al., 2016).

A multiphase hierarchical microstructure in $Al_{0.3}CoCrNi$ MEA was achieved by cold-rolling and annealing (Sathiyamoorthi et al., 2019c). After annealing, the multiphase hierarchical microstructure features non-recrystallized regions, partial recrystallized regions with fine (3 ± 2 μm) and coarse (14 ± 3 μm) grains, and hierarchical distribution of σ phase (100–500 nm) and B2 precipitates (300–400 nm). This $Al_{0.3}CoCrNi$ MEA with a multiphase hierarchical microstructure presents an excellent combination of high yield strength (1 GPa), high tensile strength (1.2 GPa), and high ductility (~28%). Similarly, the $CoCrFeNiMo_{0.3}$ HEA strengthened by σ and μ particles presents a yield strength of 816 MPa and a ductility of ~19% (Liu et al., 2016). By using different thermomechanical processings, Choudhuri et al. fabricated a three-phase microstructure consisting of FG FCC, ordered B2, and σ phase in $Al_{0.3}CoCrFeNi$ HEA (Choudhuri et al., 2019). Strikingly, the $Al_{0.3}CoCrFeNi$ HEA with a three-phase microstructure shows a fourfold increase in yield strength and more significant work hardening ability compared to that with only the FCC microstructure.

The thermomechanical processing-induced precipitations have significant effects on the mechanical properties of MEAs/HEAs. First, the precipitations promote the formation of heterogeneous grain structures. The difference in dislocation density and interface energy induced by plastic deformation results in heterogeneous nucleation and distribution of precipitation (Gwalani et al., 2018; Sathiyamoorthi et al., 2019c). Meanwhile, the heterogeneous precipitations can delay the recrystallization process and facilitate partial recrystallization with formation of fine and coarse recrystallized grains (Sathiyamoorthi et al., 2019c; He et al., 2020). Second, precipitations offer an important strengthening effect. Both the experiments by transmission electron microscopy and molecular

TABLE 6 | List of the strengthening phase (P) and mechanical properties of MEAs/HEAs reported with multiphase hierarchical microstructure.

Alloys	P	YS (MPa)	UTS (MPa)	UE (%)	References
$(FeCoNiCr)_{94}Ti_2Al_4$	$L1_2$, Ni_2AlTi	645	1,094	39	He et al. (2016)
$CoCrFeNiMo_{0.3}$	σ, μ	816	1,187	19	Liu et al. (2016)
$Al_{0.5}Cr_{0.9}FeNi_{2.5}V_{0.2}$	Ni_3Al, BCC	1800	1900	9	Liang et al. (2018)
$Al_{0.3}CrFeNi$	$L1_2$, B2	1,074	1,302	8	Dasari et al. (2020)
$Ni_{30}Co_{30}Fe_{13}Cr_{15}Al_6Ti_6$	$L1_2$	925	1,310	35	Yang et al. (2019b)
$(CoCrNi)_{94}Al_3Ti_3$	$L1_2$	750	1,300	40	Zhao et al. (2017)
$Al_{0.5}CrFeCoNiCu$	$L1_2$	850	1,300	35	Yang et al. (2018b)
$Al_7Co_{23.26}Cr_{23.26}Fe_{23.26}Ni_{23.26}$	$L1_2$, B2	490	825	48	Borkar et al. (2016)
$(Fe_{25}Co_{25}Ni_{25}Cr_{25})_{94}Ti_2Al_4$	$L1_2$, $L2_1$	645	1,094	39	He et al. (2016)
$Al_{3.7}Cr_{18.5}Fe_{18.5}Co_{18.5}Ni_{37}Cu_{3.7}$	$L1_2$	719	1,048	30.4	Wang et al. (2017)
$Al_{3.64}Co_{40.9}Cr_{27.27}Fe_{27.27}Ni_{40.9}Ti_{5.45}$	$L1_2$	640	830	10	Kuo and Tsai, (2018)
$Al_{3.31}Co_{27}Cr_{18}Fe_{18}Ni_{27.27}Ti_{5.78}$	$L1_2$	952	1,306	20.5	Chang and Yeh, (2018)
$Al_{10}Co_{25}Cr_8Fe_{15}Ni_{36}Ti_6$	$L1_2$	596	1,039	20	Daoud et al. (2015)

dynamic simulations have demonstrated that the ordered B2 and σ phases will raise the local stress levels to facilitate deformation twinning (Choudhuri et al., 2019). Furthermore, direct observation by EBSD shows the heterogeneous distribution of strain induced by the heterogeneous microstructures, with higher strain accumulation in uncrystallized regions and FGs (Sathiyamoorthi et al., 2019c). The outstanding mechanical properties of MEAs/HEAs with multiphase hierarchical microstructure are attributed to the combined effect of hierarchical constraints to the deformation of the major phase. The combination of strengthening from HDI stress induced by heterogeneous structures and effective stress induced by nano-precipitates results in high strength, while the GNDs and twins lead to a remarkable strain hardening rate and thus high ductility.

Dynamic phase transformation

It has been documented that the deformation mechanisms in FCC materials perform as a function of SFE, which can be summarized as the following: 1) SFEs for dislocation slip are higher than 60 mJm^{-2}; 2) SFEs for twinning are in the range of 20–60 mJm^{-2}; and 3) SFEs for transformation from the FCC to HCP phases are lower than 20 mJm^{-2} (Remy and Pineau, 1977; Saeed-Akbari et al., 2012). The low SFE promotes the dissociation of unit dislocation into partial dislocations and suppresses the unit dislocation slip. Furthermore, the low SFE reduces the CRSS for phase transformation, and hence it enhances the TRIP effects, leading to dynamically accumulating dislocations and hardening of alloys during deformation. Therefore, MEAs/HEAs with extremely low SFE usually experience dynamic phase transformation from FCC to HCP and achieve simultaneously enhanced strength and ductility.

Utilizing this concept, metastable dual-phase $Fe_{80-x}Mn_xCo_{10}Cr_{10}$ (at%) HEAs were developed, which overcome the traditional strength–ductility trade-off (Li et al., 2016). By tuning the Mn content, the authors realized the transition of dominating deformation mechanisms from dislocation slip to the TWIP effect in metastable HEAs, due to the lower Mn content-induced reduction of SFE. Finally, the $Fe_{50}Mn_{30}Co_{10}Cr_{10}$ HEA is composed of the dual-phase microstructure with ~28% HCP phase and ~72% FCC phase (Li et al., 2016). Upon plastic deformation, sustaining phase transformation from the FCC to HCP phases is realized through the formation of stacking faults on alternative slip planes. The phase transformation-induced high-phase boundary density creates additional obstacles for dislocation slip, thereby contributing to higher strain hardening in the dual-phase $Fe_{50}Mn_{30}Co_{10}Cr_{10}$ HEA than in the single-phase HEAs (Li et al., 2016). In conclusion, the increased interface density and the massive solid solution strengthening result in greatly improved strength, while at the same time the dislocation plasticity and transformation-induced hardening lead to enhanced ductility. The synergic deformation of the two phases leads to a highly beneficial dynamic strain–stress partitioning effect, and thus the combined increase in strength and ductility (Li et al., 2016).

Similarly, Su et al. developed an HS interstitial carbon-doped HEA ($Fe_{49.5}Mn_{30}Co_{10}Cr_{10}C_{0.5}$ (at%), which exhibits excellent mechanical properties (Su et al., 2019). Through a thermomechanical process (cold-rolling and annealing at 600°C), the authors can fine-tune the microstructures of the HEAs to form a trimodal grain structures featured by fine recrystallized grains (<1 μm) related to shear bands, medium-sized grain (1–6 μm) recrystallized from the retained FCC phase, and large non-recrystallized grains from the reverted FCC phase (**Figure 8**) (Su et al., 2019). The tri-modal grain structure shows superior combination of yield strength and ductility compared to the fully recrystallized coarse and FGs. Nano-twins and grain refinement account for the improvement in yield strength, and multistage work hardening associated with the TWIP and TRIP effects accounts for the enhanced ductility (Su et al., 2019).

The transformation nucleus of FCC usually occurs in the SF–SF intersections, which has been revealed in the FCC/BCC transformation in $Co_{25}Ni_{25}Fe_{25}Al_{7.5}Cu_{17.5}$ HEA by molecular dynamic simulation (Li et al., 2018). In addition, the nano-HCP laths may form in the presence of nano-twins, leading to the formation of nano-twin–HCP composite lamellae. The nanocomposite of the dual-phase mixture offers an optimal balance of strain and stress benefits and decreases the possibility of damage nucleation due to their elastic compliance. Without the adjustment to the deformation *via* twinning and/or dislocation slip, the deformation attributed solely to the single HCP phase transformation is prone to produce damage to the tensile specimen, thereby leading to a

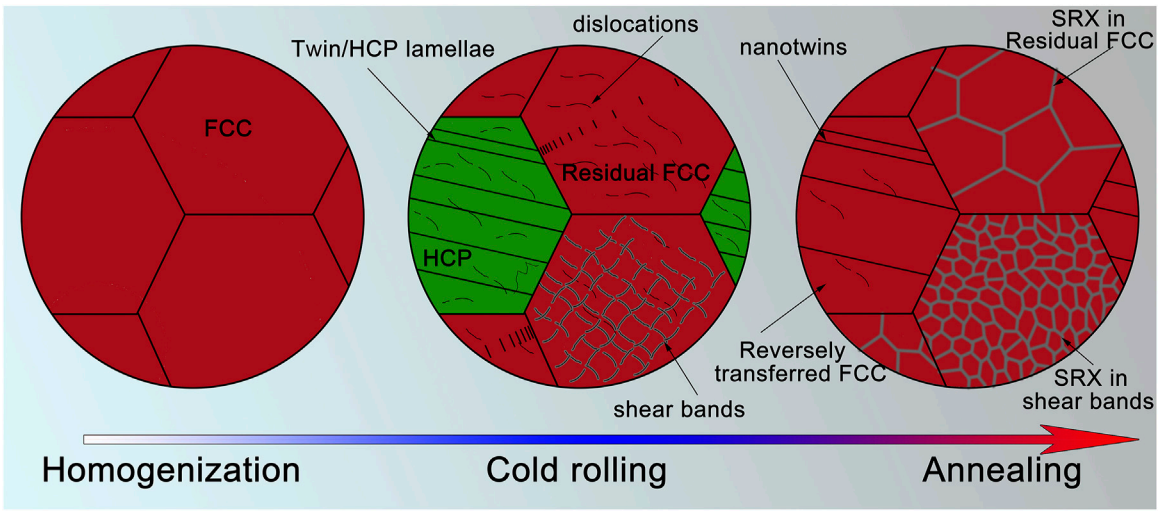

FIGURE 8 | A schematic diagram of producing $Fe_{49.5}Mn_{30}Co_{10}Cr_{10}C_{0.5}$ with bimodal and trimodal microstructures (Su et al., 2019).

premature fracture even though the TRIP effect is contributed to a high strain hardening effect. When compared with the hardening effect from TBs, the HCP lamellar structure would be an effective barrier for dislocation slip since the transmission of edge-component dislocations into the HCP phase would require the activation of either <c> or < c + a> dislocation with a component along (0001) (Miao et al., 2017; Lu et al., 2018). The <c> or < c + a> dislocation typically exhibits extremely high CRSS in HCP materials.

Heterogeneous Structure by Additive Manufacturing

The additive manufacturing technique, including selective laser melting and direct laser deposition, can also produce bulk heterogeneous structures in HEAs/MEAs, without any post-processing (e.g., homogenization, severe plastic deformation, and annealing). The additive manufacturing technique possesses unique forming mode (e.g., melt pool connection, layer-by-layer deposition, high cooling rate, and nonequilibrium solidification). Thus, the produced heterogeneous structures are usually featured by melt pools, columnar grains, cellular dislocation structures, twinning, solute heterogeneity, and precipitation (Zhu et al., 2018; Park et al., 2019; Kim et al., 2020; Luo et al., 2020; Wang et al., 2020).

In the single-phase CoCrFeMnNi HEA produced by selective laser melting, the three-dimensional dislocation network structures are observed (Zhu et al., 2018). Such unique dislocation networks generate by the substantial interaction between dislocation slip bands and cellular dislocation walls and show no misorientation with the matrix. These cellular dislocation structures can efficiently accommodate and trap dislocations to bring about remarkably dislocation hardening, thereby resulting in an outstanding combination of high strength (609 MPa) and excellent ductility (34%) (Zhu et al., 2018).

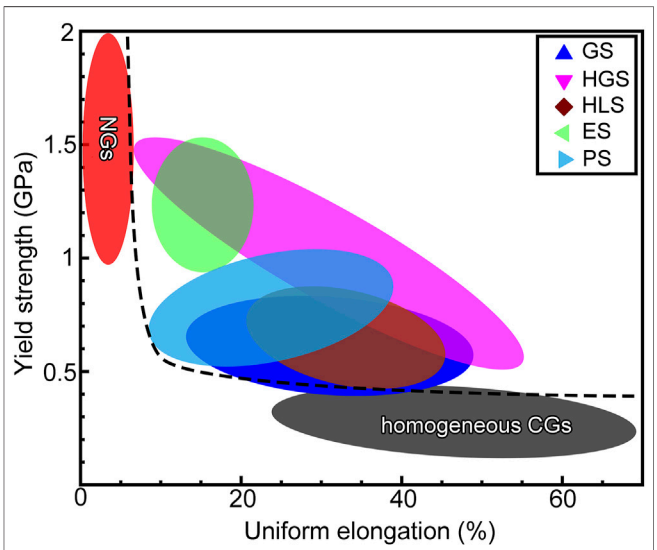

FIGURE 9 | Yield strength versus uniform elongation of MEAs/HEAs with homogeneous structures (below banana-shaped region) and various heterostructures. (GS, HGS, HLS, ES, and PS are gradient structure, heterogeneous grain structure, heterogeneous lamella structure, eutectic structure, and precipitation structure, respectively).

Luo et al. fabricate a dual-phase AlCrCuFeNix (x = 2.0, 2.5, 2.75, 3.0) HEA with BCC and FCC structures using selective laser melting (Luo et al., 2020). The AlCrCuFeNix HEA exhibits an excellent combination of strength (957 MPa) and ductility (14.3%), which is attributed to the heterogeneous microstructures and distinct deformation mechanisms in FCC and BCC phases (Luo et al., 2020). The deformation of FCC phases is carried by planar dislocation slip and stacking faults, while high densities of Cr-rich nano-precipitates promote the formation of deformation twins and stacking faults in BCC

phases. Moreover, the strain-induced phase transition from BCC to FCC contributes to the strain hardening and ductility.

However, there remains a paucity of studies on the nature and the inherent formation mechanisms of the heterogeneous structures in additively manufactured materials. Much more effort is required to understand the influence of processing parameters to design HEAs/MEAs with superior mechanical properties.

SUMMARY AND FUTURE ISSUES

This review paper introduces HS and HEA concepts and emphatically reviews the microstructure, mechanical properties, and deformation mechanisms of HS MEAs/HEAs. The HS design can enhance strain hardening capacity and delay plastic instability, effectively evading the paradox between strength and ductility observed in metallic materials with conventional strengthening strategies. The introduction of HS into MEAs/HEAs helps to achieve a superior strength–ductility synergy, as shown in **Figure 9**. The HS MEAs/HEAs should be comprised of different microstructures characterized by large strength difference, which induces stress and strain partitioning upon tensile deformation and thus leads to GND pile-up and HDI-stress effects.

From the previous reported mechanical properties of MEAs/HEAs with heterostructure, the field is still in its incipient stage and the great potential in next-generation structural and functional applications spanning diverse fields remains to be explored, such as transportation, energy sustainability (nuclear reactors and hydrogen storage), aerospace applications, and biomedical applications. Meanwhile, the shortcomings in the field of high-entropy alloy research must be faced up to, which is the transition from laboratory explorations to practical engineering applications. For example, strength and ductility are the concern for laboratory investigations whereas a complex application environment must be considered for practical applications. In this sense, more application-driven and building-up of benchmarking for commercial application is also a crucial step in exploring MEAs/HEAs. Most importantly, the expense could by and large be a decisive issue for utilizations of MEAs/HEAs, which requires careful contemplations.

AUTHOR CONTRIBUTIONS

WJ wrote the first draft of the manuscript. YTZ and YHZ reviewed and edited the manuscript. All authors contributed to the article and agreed to the submitted version of the manuscript.

FUNDING

The authors acknowledge financial support from the National Key R and D Program of China (Grant No. 2017YFA0204403), the National Natural Science Foundation of China (Grant No. 51971112 and 51225102), the Fundamental Research Funds for the Central Universities (Grant No. 30919011405), and the Hong Kong Research Grants Council (GRF 11214121).

REFERENCES

An, X. H., Wu, S. D., Zhang, Z. F., Figueiredo, R. B., Gao, N., and Langdon, T. G. (2012). Enhanced Strength-Ductility Synergy in Nanostructured Cu and Cu-Al Alloys Processed by High-Pressure Torsion and Subsequent Annealing. *Scripta Materialia* 66, 227–230. doi:10.1016/j.scriptamat.2011.10.043

Bae, J. W., Moon, J., Jang, M. J., Yim, D., Kim, D., Lee, S., et al. (2017). Trade-off between Tensile Property and Formability by Partial Recrystallization of CrMnFeCoNi High-Entropy alloy. *Mater. Sci. Eng. A* 703, 324–330. doi:10.1016/j.msea.2017.07.079

Baker, I., Meng, F., Wu, M., and Brandenberg, A. (2016). Recrystallization of a Novel Two-phase FeNiMnAlCr High Entropy alloy. *J. Alloys Compd.* 656, 458–464. doi:10.1016/j.jallcom.2015.09.264

Bhattacharjee, T., Wani, I. S., Sheikh, S., Clark, I. T., Okawa, T., Guo, S., et al. (2018). Simultaneous Strength-Ductility Enhancement of a Nano-Lamellar AlCoCrFeNi2.1 Eutectic High Entropy Alloy by Cryo-Rolling and Annealing. *Sci. Rep.* 8, 3276. doi:10.1038/s41598-018-21385-y

Bian, X., Yuan, F., Zhu, Y., and Wu, X. (2017). Gradient Structure Produces superior Dynamic Shear Properties. *Mater. Res. Lett.* 5, 501–507. doi:10.1080/21663831.2017.1334715

Borkar, T., Gwalani, B., Choudhuri, D., Mikler, C. V., Yannetta, C. J., Chen, X., et al. (2016). A Combinatorial Assessment of AlxCrCuFeNi2 (0. *Acta Materialia* 116, 63–76. doi:10.1016/j.actamat.2016.06.025

Bouaziz, O., Allain, S., Scott, C. P., Cugy, P., and Barbier, D. (2011). High Manganese Austenitic Twinning Induced Plasticity Steels: A Review of the Microstructure Properties Relationships. *Curr. Opin. Solid State. Mater. Sci.* 15, 141–168. doi:10.1016/j.cossms.2011.04.002

Bouaziz, O., Zurob, H., and Huang, M. (2013). Driving Force and Logic of Development of Advanced High Strength Steels for Automotive Applications. *Steel Research Int.* 84, a–n. doi:10.1002/srin.201200288

Byun, T. S., Hashimoto, N., and Farrell, K. (2004). Temperature Dependence of Strain Hardening and Plastic Instability Behaviors in Austenitic Stainless Steels. *Acta Materialia* 52, 3889–3899. doi:10.1016/j.actamat.2004.05.003

Calcagnotto, M., Adachi, Y., Ponge, D., and Raabe, D. (2011). Deformation and Fracture Mechanisms in fine- and Ultrafine-Grained Ferrite/martensite Dual-phase Steels and the Effect of Aging. *Acta Materialia* 59, 658–670. doi:10.1016/j.actamat.2010.10.002

Cantor, B., Chang, I. T. H., Knight, P., and Vincent, A. J. B. (2004). Microstructural Development in Equiatomic Multicomponent Alloys. *Mater. Sci. Eng. A* 375-377, 213–218. doi:10.1016/j.msea.2003.10.257

Cao, Y., Ni, S., Liao, X., Song, M., and Zhu, Y. (2018). Structural Evolutions of Metallic Materials Processed by Severe Plastic Deformation. *Mater. Sci. Eng. R: Rep.* 133, 1–59. doi:10.1016/j.mser.2018.06.001

Cao, Y., Wang, Y. B., An, X. H., Liao, X. Z., Kawasaki, M., Ringer, S. P., et al. (2014). Concurrent Microstructural Evolution of Ferrite and Austenite in a Duplex Stainless Steel Processed by High-Pressure Torsion. *Acta Materialia* 63, 16–29. doi:10.1016/j.actamat.2013.09.030

Cao, Y., Wang, Y. B., Figueiredo, R. B., Chang, L., Liao, X. Z., Kawasaki, M., et al. (2011). Three-dimensional Shear-Strain Patterns Induced by High-Pressure Torsion and Their Impact on Hardness Evolution. *Acta Materialia* 59, 3903–3914. doi:10.1016/j.actamat.2011.03.015

Chang, Y.-J., and Yeh, A.-C. (2018). The Formation of Cellular Precipitate and its Effect on the Tensile Properties of a Precipitation Strengthened High Entropy alloy. *Mater. Chem. Phys.* 210, 111–119. doi:10.1016/j.matchemphys.2017.09.057

Chen, G., Li, L. T., Qiao, J. W., Jiao, Z. M., Ma, S. G., Ng, F. L., et al. (2019a). Gradient Hierarchical Grain Structures of Al0.1CoCrFeNi High-Entropy Alloys through Dynamic Torsion. *Mater. Lett.* 238, 163–166. doi:10.1016/j.matlet.2018.11.176

Chen, G., Qiao, J. W., Jiao, Z. M., Zhao, D., Zhang, T. W., Ma, S. G., et al. (2019b). Strength-ductility Synergy of Al0.1CoCrFeNi High-Entropy Alloys with

Gradient Hierarchical Structures. *Scripta Materialia* 167, 95–100. doi:10.1016/j.scriptamat.2019.04.002

Chen, L., Cao, T., Wei, R., Tang, K., Xin, C., Jiang, F., et al. (2020). Gradient Structure Design to Strengthen Carbon Interstitial Fe40Mn40Co10Cr10 High Entropy Alloys. *Mater. Sci. Eng. A* 772, 138661. doi:10.1016/j.msea.2019.138661

Chen, X., Wang, Q., Cheng, Z., Zhu, M., Zhou, H., Jiang, P., et al. (2021). Direct Observation of Chemical Short-Range Order in a Medium-Entropy alloy. *Nature* 592, 712–716. doi:10.1038/s41586-021-03428-z

Choudhuri, D., Gwalani, B., Gorsse, S., Komarasamy, M., Mantri, S. A., Srinivasan, S. G., et al. (2019). Enhancing Strength and Strain Hardenability via Deformation Twinning in Fcc-Based High Entropy Alloys Reinforced with Intermetallic Compounds. *Acta Materialia* 165, 420–430. doi:10.1016/j.actamat.2018.12.010

Choudhuri, D., Shukla, S., Green, W. B., Gwalani, B., Ageh, V., Banerjee, R., et al. (2018). Crystallographically Degenerate B2 Precipitation in a Plastically Deformed Fcc-Based Complex Concentrated alloy. *Mater. Res. Lett.* 6, 171–177. doi:10.1080/21663831.2018.1426649

Daoud, H. M., Manzoni, A. M., Wanderka, N., and Glatzel, U. (2015). High-Temperature Tensile Strength of Al10Co25Cr8Fe15Ni36Ti6 Compositionally Complex Alloy (High-Entropy Alloy). *JOM* 67, 2271–2277. doi:10.1007/s11837-015-1484-7

Dasari, S., Gwalani, B., Jagetia, A., Soni, V., Gorsse, S., and Banerjee, R. (2020). Hierarchical Eutectoid Nano-Lamellar Decomposition in an Al0.3CoFeNi Complex Concentrated Alloy. *Sci. Rep.* 10, 4836. doi:10.1038/s41598-020-61538-6

Ding, J., Yu, Q., Asta, M., and Ritchie, R. O. (2018). Tunable Stacking Fault Energies by Tailoring Local Chemical Order in CrCoNi Medium-Entropy Alloys. *Proc. Natl. Acad. Sci. USA* 115, 8919–8924. doi:10.1073/pnas.1808660115

Ding, Q., Zhang, Y., Chen, X., Fu, X., Chen, D., Chen, S., et al. (2019). Tuning Element Distribution, Structure and Properties by Composition in High-Entropy Alloys. *Nature* 574, 223–227. doi:10.1038/s41586-019-1617-1

Dong, Y., Yao, Z., Huang, X., Du, F., Li, C., Chen, A., et al. (2020). Microstructure and Mechanical Properties of AlCoxCrFeNi3-X Eutectic High-Entropy-alloy System. *J. Alloys Compd.* 823, 153886. doi:10.1016/j.jallcom.2020.153886

Eshelby, J. D., Frank, F. C., and Nabarro, F. R. N. (1951). XLI. The Equilibrium of Linear Arrays of Dislocations. *Lond. Edinb. Dublin Philos. Mag. J. Sci.* 42, 351–364. doi:10.1080/14786445108561060

Fang, T. H., Li, W. L., Tao, N. R., and Lu, K. (2011). Revealing Extraordinary Intrinsic Tensile Plasticity in Gradient Nano-Grained Copper. *Science* 331, 1587–1590. doi:10.1126/science.1200177

Fang, X. T., He, G. Z., Zheng, C., Ma, X. L., Kaoumi, D., Li, Y. S., et al. (2020). Effect of Heterostructure and Hetero-Deformation Induced Hardening on the Strength and Ductility of Brass. *Acta Materialia* 186, 644–655. doi:10.1016/j.actamat.2020.01.037

Fu, Z., Chen, W., Wen, H., Zhang, D., Chen, Z., Zheng, B., et al. (2016). Microstructure and Strengthening Mechanisms in an FCC Structured Single-phase Nanocrystalline Co25Ni25Fe25Al7.5Cu17.5 High-Entropy alloy. *Acta Materialia* 107, 59–71. doi:10.1016/j.actamat.2016.01.050

Fu, Z., MacDonald, B. E., Zhang, D., Wu, B., Chen, W., Ivanisenko, J., et al. (2018). Fcc Nanostructured TiFeCoNi alloy with Multi-Scale Grains and Enhanced Plasticity. *Scripta Materialia* 143, 108–112. doi:10.1016/j.scriptamat.2017.09.023

Gao, B., Lai, Q., Cao, Y., Hu, R., Xiao, L., Pan, Z., et al. (2020). Ultrastrong Low-Carbon Nanosteel Produced by Heterostructure and Interstitial Mediated Warm Rolling. *Sci. Adv.* 6, eaba8169. doi:10.1126/sciadv.aba8169

Gao, X., Lu, Y., Liu, J., Wang, J., Wang, T., and Zhao, Y. (2019). Extraordinary Ductility and Strain Hardening of Cr26Mn20Fe20Co20Ni14 TWIP High-Entropy alloy by Cooperative Planar Slipping and Twinning. *Materialia* 8, 100485. doi:10.1016/j.mtla.2019.100485

Gao, X., Lu, Y., Zhang, B., Liang, N., Wu, G., Sha, G., et al. (2017). Microstructural Origins of High Strength and High Ductility in an AlCoCrFeNi2.1 Eutectic High-Entropy alloy. *Acta Materialia* 141, 59–66. doi:10.1016/j.actamat.2017.07.041

Gludovatz, B., Hohenwarter, A., Catoor, D., Chang, E. H., George, E. P., and Ritchie, R. O. (2014). A Fracture-Resistant High-Entropy alloy for Cryogenic Applications. *Science* 345, 1153–1158. doi:10.1126/science.1254581

Gludovatz, B., Hohenwarter, A., Thurston, K. V. S., Bei, H., Wu, Z., George, E. P., et al. (2016). Exceptional Damage-Tolerance of a Medium-Entropy alloy CrCoNi at Cryogenic Temperatures. *Nat. Commun.* 7, 10602. doi:10.1038/ncomms10602

Grässel, O., Krüger, L., Frommeyer, G., and Meyer, L. W. (2000). High Strength Fe–Mn–(Al, Si) TRIP/TWIP Steels Development — Properties — Application. *Int. J. Plast.* 16, 1391–1409. doi:10.1016/S0749-6419(00)00015-2

Guo, L., Wu, W., Ni, S., Yuan, Z., Cao, Y., Wang, Z., et al. (2020). Strengthening the FeCoCrNiMo0.15 High Entropy alloy by a Gradient Structure. *J. Alloys Compd.* 841, 155688. doi:10.1016/j.jallcom.2020.155688

Gutierrez-Urrutia, I., and Raabe, D. (2011). Dislocation and Twin Substructure Evolution during Strain Hardening of an Fe–22wt.% Mn–0.6wt.% C TWIP Steel Observed by Electron Channeling Contrast Imaging. *Acta Mater.* 59, 6449–6462. doi:10.1016/j.actamat.2011.07.009

Gutierrez-Urrutia, I., and Raabe, D. (2012). Grain Size Effect on Strain Hardening in Twinning-Induced Plasticity Steels. *Scripta Materialia* 66, 992–996. doi:10.1016/j.scriptamat.2012.01.037

Gwalani, B., Gorsse, S., Choudhuri, D., Styles, M., Zheng, Y., Mishra, R. S., et al. (2018). Modifying Transformation Pathways in High Entropy Alloys or Complex Concentrated Alloys via Thermo-Mechanical Processing. *Acta Materialia* 153, 169–185. doi:10.1016/j.actamat.2018.05.009

Han, B. O., Lavernia, E. J., Lee, Z., Nutt, S., and Witkin, D. (2005). Deformation Behavior of Bimodal Nanostructured 5083 Al Alloys. *Metall. Mat Trans. A.* 36, 957–965. doi:10.1007/s11661-005-0289-7

Han, Z. H., Liang, S., Yang, J., Wei, R., and Zhang, C. J. (2018). A superior Combination of Strength-Ductility in CoCrFeNiMn High-Entropy alloy Induced by Asymmetric Rolling and Subsequent Annealing Treatment. *Mater. Characterization* 145, 619–626. doi:10.1016/j.matchar.2018.09.029

Hansen, N. (2004). Hall-Petch Relation and Boundary Strengthening. *Scripta Materialia* 51, 801–806. doi:10.1016/j.scriptamat.2004.06.002

Hart, E. W. (1967). Theory of the Tensile Test. *Acta Metallurgica* 15, 351–355. doi:10.1016/0001-6160(67)90211-8

Hasan, M. N., Liu, Y. F., An, X. H., Gu, J., Song, M., Cao, Y., et al. (2019). Simultaneously Enhancing Strength and Ductility of a High-Entropy alloy via Gradient Hierarchical Microstructures. *Int. J. Plasticity* 123, 178–195. doi:10.1016/j.ijplas.2019.07.017

He, B. B., Hu, B., Yen, H. W., Cheng, G. J., Wang, Z. K., Luo, H. W., et al. (2017). High Dislocation Density-Induced Large Ductility in Deformed and Partitioned Steels. *Science* 357, 1029–1032. doi:10.1126/science.aan0177

He, J., Makineni, S. K., Lu, W., Shang, Y., Lu, Z., Li, Z., et al. (2020). On the Formation of Hierarchical Microstructure in a Mo-Doped NiCoCr Medium-Entropy alloy with Enhanced Strength-Ductility Synergy. *Scripta Materialia* 175, 1–6. doi:10.1016/j.scriptamat.2019.08.036

He, J. Y., Wang, H., Wu, Y., Liu, X. J., Mao, H. H., Nieh, T. G., et al. (2016). Precipitation Behavior and its Effects on Tensile Properties of FeCoNiCr High-Entropy Alloys. *Intermetallics* 79, 41–52. doi:10.1016/j.intermet.2016.09.005

Huang, C. X., Wang, Y. F., Ma, X. L., Yin, S., Höppel, H. W., Göken, M., et al. (2018). Interface Affected Zone for Optimal Strength and Ductility in Heterogeneous Laminate. *Mater. Today* 21, 713–719. doi:10.1016/j.mattod.2018.03.006

Huang, K., Zhang, K., Marthinsen, K., and Logé, R. E. (2017). Controlling Grain Structure and Texture in Al-Mn from the Competition between Precipitation and Recrystallization. *Acta Materialia* 141, 360–373. doi:10.1016/j.actamat.2017.09.032

Hughes, D. A., Hansen, N., and Bammann, D. J. (2003). Geometrically Necessary Boundaries, Incidental Dislocation Boundaries and Geometrically Necessary Dislocations. *Scripta Materialia* 48, 147–153. doi:10.1016/S1359-6462(02)00358-5

Jiang, W., Cao, Y., Jiang, Y., Liu, Y., Mao, Q., Zhou, H., et al. (2021a). Effects of Nanostructural Hierarchy on the Hardness and thermal Stability of an Austenitic Stainless Steel. *J. Mater. Res. Techn.* 12, 376–384. doi:10.1016/j.jmrt.2021.02.100

Jiang, W., Gao, X., Guo, Y., Chen, X., and Zhao, Y. (2021b). Dynamic Impact Behavior and Deformation Mechanisms of Cr26Mn20Fe20Co20Ni14 High-Entropy alloy. *Mater. Sci. Eng. A* 824, 141858. doi:10.1016/j.msea.2021.141858

Jiang, W., Yuan, S., Cao, Y., Zhang, Y., and Zhao, Y. (2021c). Mechanical Properties and Deformation Mechanisms of a Ni2Co1Fe1V0.5Mo0.2 Medium-Entropy

alloy at Elevated Temperatures. *Acta Materialia* 213, 116982. doi:10.1016/j.actamat.2021.116982

Jin, X., Bi, J., Zhang, L., Zhou, Y., Du, X., Liang, Y., et al. (2019). A New CrFeNi2Al Eutectic High Entropy alloy System with Excellent Mechanical Properties. *J. Alloys Compd.* 770, 655–661. doi:10.1016/j.jallcom.2018.08.176

Jin, X., Zhou, Y., Zhang, L., Du, X., and Li, B. (2018a). A New Pseudo Binary Strategy to Design Eutectic High Entropy Alloys Using Mixing Enthalpy and Valence Electron Concentration. *Mater. Des.* 143, 49–55. doi:10.1016/j.matdes.2018.01.057

Jin, X., Zhou, Y., Zhang, L., Du, X., and Li, B. (2018b). A Novel Fe 20 Co 20 Ni 41 Al 19 Eutectic High Entropy alloy with Excellent Tensile Properties. *Mater. Lett.* 216, 144–146. doi:10.1016/j.matlet.2018.01.017

Jo, Y. H., Jung, S., Choi, W. M., Sohn, S. S., Kim, H. S., Lee, B. J., et al. (2017). Cryogenic Strength Improvement by Utilizing Room-Temperature Deformation Twinning in a Partially Recrystallized VCrMnFeCoNi High-Entropy alloy. *Nat. Commun.* 8, 15719. doi:10.1038/ncomms15719

Kim, J. G., Park, J. M., Seol, J. B., Choe, J., Yu, J.-H., Yang, S., et al. (2020). Nano-scale Solute Heterogeneities in the Ultrastrong Selectively Laser Melted Carbon-Doped CoCrFeMnNi alloy. *Mater. Sci. Eng. A* 773, 138726. doi:10.1016/j.msea.2019.138726

Kuo, C.-M., and Tsai, C.-W. (2018). Effect of Cellular Structure on the Mechanical Property of Al0.2Co1.5CrFeNi1.5Ti0.3 High-Entropy alloy. *Mater. Chem. Phys.* 210, 103–110. doi:10.1016/j.matchemphys.2017.10.064

Li, H., Mao, Q., Wang, Z., Miao, F., Fang, B., and Zheng, Z. (2015). Enhancing Mechanical Properties of Al-Mg-Si-Cu Sheets by Solution Treatment Substituting for Recrystallization Annealing before the Final Cold-Rolling. *Mater. Sci. Eng. A* 620, 204–212. doi:10.1016/j.msea.2014.10.012

Li, J., Fang, C., Liu, Y., Huang, Z., Wang, S., Mao, Q., et al. (2019a). Deformation Mechanisms of 304L Stainless Steel with Heterogeneous Lamella Structure. *Mater. Sci. Eng. A* 742, 409–413. doi:10.1016/j.msea.2018.11.047

Li, J., Fang, Q., Liu, B., and Liu, Y. (2018). Transformation Induced Softening and Plasticity in High Entropy Alloys. *Acta Materialia* 147, 35–41. doi:10.1016/j.actamat.2018.01.002

Li, J., Weng, G. J., Chen, S., and Wu, X. (2017). On Strain Hardening Mechanism in Gradient Nanostructures. *Int. J. Plasticity* 88, 89–107. doi:10.1016/j.ijplas.2016.10.003

Li, Q.-J., Sheng, H., and Ma, E. (2019b). Strengthening in Multi-Principal Element Alloys with Local-Chemical-Order Roughened Dislocation Pathways. *Nat. Commun.* 10, 3563. doi:10.1038/s41467-019-11464-7

Li, W. L., Tao, N. R., and Lu, K. (2008). Fabrication of a Gradient Nano-Micro-Structured Surface Layer on Bulk Copper by Means of a Surface Mechanical Grinding Treatment. *Scripta Materialia* 59, 546–549. doi:10.1016/j.scriptamat.2008.05.003

Li, W., Xie, D., Li, D., Zhang, Y., Gao, Y., and Liaw, P. K. (2021). Mechanical Behavior of High-Entropy Alloys. *Prog. Mater. Sci.* 118, 100777. doi:10.1016/j.pmatsci.2021.100777

Li, X., Wei, Y., Lu, L., Lu, K., and Gao, H. (2010). Dislocation Nucleation Governed Softening and Maximum Strength in Nano-Twinned Metals. *Nature* 464, 877–880. doi:10.1038/nature08929

Li, Z., Pradeep, K. G., Deng, Y., Raabe, D., and Tasan, C. C. (2016). Metastable High-Entropy Dual-phase Alloys Overcome the Strength-Ductility Trade-Off. *Nature* 534, 227–230. doi:10.1038/nature17981

Liang, N., Wang, X., Cao, Y., Li, Y., Zhu, Y., and Zhao, Y. (2020). Effective Surface Nano-Crystallization of Ni2FeCoMo0.5V0.2 Medium Entropy Alloy by Rotationally Accelerated Shot Peening (RASP). *Entropy* 22, 1074. doi:10.3390/e22101074

Liang, Y.-J., Wang, L., Wen, Y., Cheng, B., Wu, Q., Cao, T., et al. (2018). High-content Ductile Coherent Nanoprecipitates Achieve Ultrastrong High-Entropy Alloys. *Nat. Commun.* 9, 4063. doi:10.1038/s41467-018-06600-8

Liu, J., Chen, Z., Zhang, F., Ji, G., Wang, M., Ma, Y., et al. (2018). Simultaneously Increasing Strength and Ductility of Nanoparticles Reinforced Al Composites via Accumulative Orthogonal Extrusion Process. *Mater. Res. Lett.* 6, 406–412. doi:10.1080/21663831.2018.1471421

Liu, W. H., Lu, Z. P., He, J. Y., Luan, J. H., Wang, Z. J., Liu, B., et al. (2016). Ductile CoCrFeNiMox High Entropy Alloys Strengthened by Hard Intermetallic Phases. *Acta Materialia* 116, 332–342. doi:10.1016/j.actamat.2016.06.063

Liu, Y., Cao, Y., Mao, Q., Zhou, H., Zhao, Y., Jiang, W., et al. (2020). Critical Microstructures and Defects in Heterostructured Materials and Their Effects on Mechanical Properties. *Acta Materialia* 189, 129–144. doi:10.1016/j.actamat.2020.03.001

Liu, Y., He, Y., and Cai, S. (2021a). Effect of Gradient Microstructure on the Strength and Ductility of Medium-Entropy alloy Processed by Severe Torsion Deformation. *Mater. Sci. Eng. A* 801, 140429. doi:10.1016/j.msea.2020.140429

Liu, Y., He, Y., and Cai, S. (2021b). Gradient Recrystallization to Improve Strength and Ductility of Medium-Entropy alloy. *J. Alloys Compd.* 853, 157388. doi:10.1016/j.jallcom.2020.157388

Lu, K., Lu, L., and Suresh, S. (2009a). Strengthening Materials by Engineering Coherent Internal Boundaries at the Nanoscale. *Science* 324, 349–352. doi:10.1126/science.1159610

Lu, K. (2014). Making strong Nanomaterials Ductile with Gradients. *Science* 345, 1455–1456. doi:10.1126/science.1255940

Lu, L., Chen, X., Huang, X., and Lu, K. (2009b). Revealing the Maximum Strength in Nanotwinned Copper. *Science* 323, 607–610. doi:10.1126/science.1167641

Lu, L., Shen, Y., Chen, X., Qian, L., and Lu, K. (2004). Ultrahigh Strength and High Electrical Conductivity in Copper. *Science* 304, 422–426. doi:10.1126/science.1092905

Lu, W., Liebscher, C. H., Dehm, G., Raabe, D., and Li, Z. (2018). Bidirectional Transformation Enables Hierarchical Nanolaminate Dual-phase High-Entropy Alloys. *Adv. Mater.* 30, 1804727. doi:10.1002/adma.201804727

Lu, Y., Dong, Y., Guo, S., Jiang, L., Kang, H., Wang, T., et al. (2014). A Promising New Class of High-Temperature Alloys: Eutectic High-Entropy Alloys. *Sci. Rep.* 4, 6200. doi:10.1038/srep06200

Lucas, M. S., Wilks, G. B., Mauger, L., Muñoz, J. A., Senkov, O. N., Michel, E., et al. (2012). Absence of Long-Range Chemical Ordering in Equimolar FeCoCrNi. *Appl. Phys. Lett.* 100, 251907. doi:10.1063/1.4730327

Luo, S., Zhao, C., Su, Y., Liu, Q., and Wang, Z. (2020). Selective Laser Melting of Dual Phase AlCrCuFeNix High Entropy Alloys: Formability, Heterogeneous Microstructures and Deformation Mechanisms. *Additive Manufacturing* 31, 100925. doi:10.1016/j.addma.2019.100925

Ma, E., and Zhu, T. (2017). Towards Strength-Ductility Synergy through the Design of Heterogeneous Nanostructures in Metals. *Mater. Today* 20, 323–331. doi:10.1016/j.mattod.2017.02.003

Ma, X., Huang, C., Moering, J., Ruppert, M., Höppel, H. W., Göken, M., et al. (2016). Mechanical Properties of Copper/bronze Laminates: Role of Interfaces. *Acta Materialia* 116, 43–52. doi:10.1016/j.actamat.2016.06.023

Mao, Q., Chen, X., Li, J., and Zhao, Y. (2021). Nano-Gradient Materials Prepared by Rotary Swaging. *Nanomaterials* 11, 2223. doi:10.3390/nano11092223

Meyers, M. A., and Chawla, K. K. (2008). *Mechanical Behavior of Materials*. Cambridge University Press. doi:10.1016/S1369-7021(09)70086-0

Miao, J., Slone, C. E., Smith, T. M., Niu, C., Bei, H., Ghazisaeidi, M., et al. (2017). The Evolution of the Deformation Substructure in a Ni-Co-Cr Equiatomic Solid Solution alloy. *Acta Materialia* 132, 35–48. doi:10.1016/j.actamat.2017.04.033

Ming, K., Bi, X., and Wang, J. (2017). Precipitation Strengthening of Ductile Cr 15 Fe 20 Co 35 Ni 20 Mo 10 Alloys. *Scripta Materialia* 137, 88–93. doi:10.1016/j.scriptamat.2017.05.019

Ming, K., Bi, X., and Wang, J. (2019). Strength and Ductility of CrFeCoNiMo alloy with Hierarchical Microstructures. *Int. J. Plasticity* 113, 255–268. doi:10.1016/j.ijplas.2018.10.005

Miracle, D. B., and Senkov, O. N. (2017). A Critical Review of High Entropy Alloys and Related Concepts. *Acta Materialia* 122, 448–511. doi:10.1016/j.actamat.2016.08.081

Miracle, D., Miller, J., Senkov, O., Woodward, C., Uchic, M., and Tiley, J. (2014). Exploration and Development of High Entropy Alloys for Structural Applications. *Entropy* 16, 494–525. doi:10.3390/e16010494

Moering, J., Ma, X., Malkin, J., Yang, M., Zhu, Y., and Mathaudhu, S. (2016). Synergetic Strengthening Far beyond Rule of Mixtures in Gradient Structured Aluminum Rod. *Scripta Materialia* 122, 106–109. doi:10.1016/j.scriptamat.2016.05.006

Olevsky, E. A., and Froyen, L. (2009). Impact of Thermal Diffusion on Densification during SPS. *J. Am. Ceram. Soc.* 92, S122–S132. doi:10.1111/j.1551-2916.2008.02705.x

Pan, Q., Zhang, L., Feng, R., Lu, Q., An, K., Chuang, A. C., et al. (2021). Gradientcell-Structured High-Entropy Alloy with Exceptional Strength and Ductility. *Science* 374, 984–989. doi:10.1126/science.abj8114

Park, J. M., Choe, J., Kim, J. G., Bae, J. W., Moon, J., Yang, S., et al. (2019). Superior Tensile Properties of 1%C-CoCrFeMnNi High-Entropy alloy Additively

Manufactured by Selective Laser Melting. *Mater. Res. Lett.* 8, 1–7. doi:10.1080/21663831.2019.1638844

Qin, W., Mao, Q., Kang, J., Liu, Y., Shu, D., She, D., et al. (2019). Superior Impact Property and Fracture Mechanism of a Multilayered Copper/bronze Laminate. *Mater. Lett.* 250, 60–63. doi:10.1016/j.matlet.2019.04.119

Reddy, S. R., Yoshida, S., Sunkari, U., Lozinko, A., Joseph, J., Saha, R., et al. (2019). Engineering Heterogeneous Microstructure by Severe Warm-Rolling for Enhancing Strength-Ductility Synergy in Eutectic High Entropy Alloys. *Mater. Sci. Eng. A* 764, 138226. doi:10.1016/j.msea.2019.138226

Remy, L., and Pineau, A. (1977). Twinning and Strain-Induced F.C.C. → H.C.P. Transformation in the Fe Mn Cr C System. *Mater. Sci. Eng.* 28, 99–107. doi:10.1016/0025-5416(77)90093-3

Ritchie, R. O. (2011). The Conflicts between Strength and Toughness. *Nat. Mater* 10, 817–822. doi:10.1038/nmat3115

Saeed-Akbari, A., Mosecker, L., Schwedt, A., and Bleck, W. (2012). Characterization and Prediction of Flow Behavior in High-Manganese Twinning Induced Plasticity Steels: Part I. Mechanism Maps and Work-Hardening Behavior. *Metall. Mat Trans. A.* 43, 1688–1704. doi:10.1007/s11661-011-0993-4

Sathiyamoorthi, P., Asghari-Rad, P., Bae, J. W., and Kim, H. S. (2019a). Fine Tuning of Tensile Properties in CrCoNi Medium Entropy alloy through Cold Rolling and Annealing. *Intermetallics* 113, 106578. doi:10.1016/j.intermet.2019.106578

Sathiyamoorthi, P., and Kim, H. S. (2022). High-entropy Alloys with Heterogeneous Microstructure: Processing and Mechanical Properties. *Prog. Mater. Sci.* 123, 100709. doi:10.1016/j.pmatsci.2020.100709

Sathiyamoorthi, P., Moon, J., Bae, J. W., Asghari-Rad, P., and Kim, H. S. (2019b). Superior Cryogenic Tensile Properties of Ultrafine-Grained CoCrNi Medium-Entropy alloy Produced by High-Pressure Torsion and Annealing. *Scripta Materialia* 163, 152–156. doi:10.1016/j.scriptamat.2019.01.016

Sathiyamoorthi, P., Park, J. M., Moon, J., Bae, J. W., Asghari-Rad, P., Zargaran, A., et al. (2019c). Achieving High Strength and High Ductility in Al0.3CoCrNi Medium-Entropy alloy through Multi-phase Hierarchical Microstructure. *Materialia* 8, 100442. doi:10.1016/j.mtla.2019.100442

Sawangrat, C., Kato, S., Orlov, D., and Ameyama, K. (2014). Harmonic-structured Copper: Performance and Proof of Fabrication Concept Based on Severe Plastic Deformation of Powders. *J. Mater. Sci.* 49, 6579–6585. doi:10.1007/s10853-014-8258-4

Schuh, B., Pippan, R., and Hohenwarter, A. (2019). Tailoring Bimodal Grain Size Structures in Nanocrystalline Compositionally Complex Alloys to Improve Ductility. *Mater. Sci. Eng. A* 748, 379–385. doi:10.1016/j.msea.2019.01.073

Senkov, O. N., Wilks, G. B., Scott, J. M., and Miracle, D. B. (2011). Mechanical Properties of Nb25Mo25Ta25W25 and V20Nb20Mo20Ta20W20 Refractory High Entropy Alloys. *Intermetallics* 19, 698–706. doi:10.1016/j.intermet.2011.01.004

Shahmir, H., He, J., Lu, Z., Kawasaki, M., and Langdon, T. G. (2016). Effect of Annealing on Mechanical Properties of a Nanocrystalline CoCrFeNiMn High-Entropy alloy Processed by High-Pressure Torsion. *Mater. Sci. Eng. A* 676, 294–303. doi:10.1016/j.msea.2016.08.118

Shi, P., Li, R., Li, Y., Wen, Y., Zhong, Y., Ren, W., et al. (2021). Hierarchical Crack Buffering Triples Ductility in Eutectic Herringbone High-Entropy Alloys. *Science* 373, 912–918. doi:10.1126/science.abf6986

Shi, P., Ren, W., Zheng, T., Ren, Z., Hou, X., Peng, J., et al. (2019). Enhanced Strength-Ductility Synergy in Ultrafine-Grained Eutectic High-Entropy Alloys by Inheriting Microstructural Lamellae. *Nat. Commun.* 10, 489. doi:10.1038/s41467-019-08460-2

Shukla, S., Wang, T., Cotton, S., and Mishra, R. S. (2018). Hierarchical Microstructure for Improved Fatigue Properties in a Eutectic High Entropy alloy. *Scripta Materialia* 156, 105–109. doi:10.1016/j.scriptamat.2018.07.022

Slone, C. E., Miao, J., George, E. P., and Mills, M. J. (2019). Achieving Ultra-high Strength and Ductility in Equiatomic CrCoNi with Partially Recrystallized Microstructures. *Acta Materialia* 165, 496–507. doi:10.1016/j.actamat.2018.12.015

Song, H., Tian, F., Hu, Q.-M., Vitos, L., Wang, Y., Shen, J., et al. (2017). Local Lattice Distortion in High-Entropy Alloys. *Phys. Rev. Mater.* 1, 023404. doi:10.1103/PhysRevMaterials.1.023404

Su, J., Raabe, D., and Li, Z. (2019). Hierarchical Microstructure Design to Tune the Mechanical Behavior of an Interstitial TRIP-TWIP High-Entropy alloy. *Acta Materialia* 163, 40–54. doi:10.1016/j.actamat.2018.10.017

Taylor, G. I. (1934). The Mechanism of Plastic Deformation of Crystals. Part I. Theoretical. *Proc. R. Soc. A.* 145, 362–387. doi:10.1016/0001-6160(81)90112-7

Tsai, K.-Y., Tsai, M.-H., and Yeh, J.-W. (2013). Sluggish Diffusion in Co-cr-fe-mn-ni High-Entropy Alloys. *Acta Materialia* 61, 4887–4897. doi:10.1016/j.actamat.2013.04.058

Tsai, M.-H., and Yeh, J.-W. (2014). High-Entropy Alloys: A Critical Review. *Mater. Res. Lett.* 2, 107–123. doi:10.1080/21663831.2014.912690

Wang, H., Zhu, Z. G., Chen, H., Wang, A. G., Liu, J. Q., Liu, H. W., et al. (2020). Effect of Cyclic Rapid thermal Loadings on the Microstructural Evolution of a CrMnFeCoNi High-Entropy alloy Manufactured by Selective Laser Melting. *Acta Materialia* 196, 609–625. doi:10.1016/j.actamat.2020.07.006

Wang, T., Shukla, S., Komarasamy, M., Liu, K., and Mishra, R. S. (2019). Towards Heterogeneous AlxCoCrFeNi High Entropy alloy via Friction Stir Processing. *Mater. Lett.* 236, 472–475. doi:10.1016/j.matlet.2018.10.161

Wang, Y., Chen, M., Zhou, F., and Ma, E. (2002). High Tensile Ductility in a Nanostructured Metal. *Nature* 419, 912–915. doi:10.1038/nature01133

Wang, Y. M., and Ma, E. (2004). Three Strategies to Achieve Uniform Tensile Deformation in a Nanostructured Metal. *Acta Materialia* 52, 1699–1709. doi:10.1016/j.actamat.2003.12.022

Wang, Z. G., Zhou, W., Fu, L. M., Wang, J. F., Luo, R. C., Han, X. C., et al. (2017). Effect of Coherent L12 Nanoprecipitates on the Tensile Behavior of a Fcc-Based High-Entropy alloy. *Mater. Sci. Eng. A* 696, 503–510. doi:10.1016/j.msea.2017.04.111

Wang, Z., Wu, M., Cai, Z., Chen, S., and Baker, I. (2016). Effect of Ti Content on the Microstructure and Mechanical Behavior of (Fe36Ni18Mn33Al13)100−xTix High Entropy Alloys. *Intermetallics* 75, 79–87. doi:10.1016/j.intermet.2016.06.001

Wei, Q., Cheng, S., Ramesh, K. T., and Ma, E. (2004). Effect of Nanocrystalline and Ultrafine Grain Sizes on the Strain Rate Sensitivity and Activation Volume: Fcc versus Bcc Metals. *Mater. Sci. Eng. A* 381, 71–79. doi:10.1016/j.msea.2004.03.064

Wei, Y., Li, Y., Zhu, L., Liu, Y., Lei, X., Wang, G., et al. (2014). Evading the Strength-Ductility Trade-Off Dilemma in Steel through Gradient Hierarchical Nanotwins. *Nat. Commun.* 5, 3580. doi:10.1038/ncomms4580

Wu, Q., Wang, Z., Zheng, T., Chen, D., Yang, Z., Li, J., et al. (2019a). A Casting Eutectic High Entropy alloy with superior Strength-Ductility Combination. *Mater. Lett.* 253, 268–271. doi:10.1016/j.matlet.2019.06.067

Wu, S. W., Wang, G., Wang, Q., Jia, Y. D., Yi, J., Zhai, Q. J., et al. (2019b). Enhancement of Strength-Ductility Trade-Off in a High-Entropy alloy through a Heterogeneous Structure. *Acta Materialia* 165, 444–458. doi:10.1016/j.actamat.2018.12.012

Wu, W., Guo, L., Liu, B., Ni, S., Liu, Y., and Song, M. (2017). Effects of Torsional Deformation on the Microstructures and Mechanical Properties of a CoCrFeNiMo0.15 High-Entropy alloy. *Philos. Mag.* 97, 3229–3245. doi:10.1080/14786435.2017.1369191

Wu, X., Jiang, P., Chen, L., Yuan, F., and Zhu, Y. T. (2014a). Extraordinary Strain Hardening by Gradient Structure. *Proc. Natl. Acad. Sci.* 111, 7197–7201. doi:10.1073/pnas.1324069111

Wu, X. L., Jiang, P., Chen, L., Zhang, J. F., Yuan, F. P., and Zhu, Y. T. (2014b). Synergetic Strengthening by Gradient Structure. *Mater. Res. Lett.* 2, 185–191. doi:10.1080/21663831.2014.935821

Wu, X., Yang, M., Yuan, F., Wu, G., Wei, Y., Huang, X., et al. (2015). Heterogeneous Lamella Structure Unites Ultrafine-Grain Strength with Coarse-Grain Ductility. *Proc. Natl. Acad. Sci. USA* 112, 14501–14505. doi:10.1073/pnas.1517193112

Wu, X., and Zhu, Y. (2021). Gradient and Lamellar Heterostructures for superior Mechanical Properties. *MRS Bull.* 46, 244–249. doi:10.1557/s43577-021-00056-w

Wu, X., and Zhu, Y. (2017). Heterogeneous Materials: a New Class of Materials with Unprecedented Mechanical Properties. *Mater. Res. Lett.* 5, 527–532. doi:10.1080/21663831.2017.1343208

Xie, J., Zhang, S., Sun, Y., Hao, Y., An, B., Li, Q., et al. (2020a). Microstructure and Mechanical Properties of High Entropy CrMnFeCoNi alloy Processed by Electopulsing-Assisted Ultrasonic Surface Rolling. *Mater. Sci. Eng. A* 795, 140004. doi:10.1016/j.msea.2020.140004

Xie, Y., Liang, J., Zhang, D., Luo, Y., Zhang, Z., Liu, Y., et al. (2020b). Sustaining Strength-Ductility Synergy of CoCrFeNiMn High Entropy alloy by a Multilevel

Heterogeneity Associated with Nanoparticles. *Scripta Materialia* 187, 390–394. doi:10.1016/j.scriptamat.2020.06.054

Xiong, T., Zheng, S., Pang, J., and Ma, X. (2020). High-strength and High-Ductility AlCoCrFeNi2.1 Eutectic High-Entropy alloy Achieved via Precipitation Strengthening in a Heterogeneous Structure. *Scripta Materialia* 186, 336–340. doi:10.1016/j.scriptamat.2020.04.035

Yang, M., Pan, Y., Yuan, F., Zhu, Y., and Wu, X. (2016). Back Stress Strengthening and Strain Hardening in Gradient Structure. *Mater. Res. Lett.* 4, 145–151. doi:10.1080/21663831.2016.1153004

Yang, M., Yan, D., Yuan, F., Jiang, P., Ma, E., and Wu, X. (2018a). Dynamically Reinforced Heterogeneous Grain Structure Prolongs Ductility in a Medium-Entropy alloy with Gigapascal Yield Strength. *Proc. Natl. Acad. Sci. USA* 115, 7224–7229. doi:10.1073/pnas.1807817115

Yang, M., Zhou, L., Wang, C., Jiang, P., Yuan, F., Ma, E., et al. (2019a). High Impact Toughness of CrCoNi Medium-Entropy alloy at Liquid-Helium Temperature. *Scripta Materialia* 172, 66–71. doi:10.1016/j.scriptamat.2019.07.010

Yang, T., Zhao, Y., Liu, W., Kai, J., and Liu, C. (2018b). L12-strengthened High-Entropy Alloys for Advanced Structural Applications. *J. Mater. Res.* 33, 2983–2997. doi:10.1557/jmr.2018.186

Yang, T., Zhao, Y. L., Luan, J. H., Han, B., Wei, J., Kai, J. J., et al. (2019b). Nanoparticles-strengthened High-Entropy Alloys for Cryogenic Applications Showing an Exceptional Strength-Ductility Synergy. *Scripta Materialia* 164, 30–35. doi:10.1016/j.scriptamat.2019.01.034

Yang, X., Ma, X., Moering, J., Zhou, H., Wang, W., Gong, Y., et al. (2015). Influence of Gradient Structure Volume Fraction on the Mechanical Properties of Pure Copper. *Mater. Sci. Eng. A* 645, 280–285. doi:10.1016/j.msea.2015.08.037

Yeh, J.-W., Chang, S.-Y., Hong, Y.-D., Chen, S.-K., and Lin, S.-J. (2007). Anomalous Decrease in X-ray Diffraction Intensities of Cu-Ni-Al-Co-Cr-Fe-Si alloy Systems with Multi-Principal Elements. *Mater. Chem. Phys.* 103, 41–46. doi:10.1016/j.matchemphys.2007.01.003

Yeh, J.-W., Chen, S.-K., Lin, S.-J., Gan, J.-Y., Chin, T.-S., Shun, T.-T., et al. (2004). Nanostructured High-Entropy Alloys with Multiple Principal Elements: Novel Alloy Design Concepts and Outcomes. *Adv. Eng. Mater.* 6, 299–303. doi:10.1002/adem.200300567

Zaddach, A. J., Niu, C., Koch, C. C., and Irving, D. L. (2013). Mechanical Properties and Stacking Fault Energies of NiFeCrCoMn High-Entropy alloy. *JOM* 65, 1780–1789. doi:10.1007/s11837-013-0771-4

Zhang, C., Zhu, C., Cao, P., Wang, X., Ye, F., Kaufmann, K., et al. (2020). Aged Metastable High-Entropy Alloys with Heterogeneous Lamella Structure for superior Strength-Ductility Synergy. *Acta Materialia* 199, 602–612. doi:10.1016/j.actamat.2020.08.043

Zhang, C., Zhu, C., Harrington, T., and Vecchio, K. (2018). Design of Non-equiatomic High Entropy Alloys with Heterogeneous Lamella Structure towards Strength-Ductility Synergy. *Scripta Materialia* 154, 78–82. doi:10.1016/j.scriptamat.2018.05.020

Zhang, C., Zhu, C., and Vecchio, K. (2019). Non-equiatomic FeNiCoAl-Based High Entropy Alloys with Multiscale Heterogeneous Lamella Structure for Strength and Ductility. *Mater. Sci. Eng. A* 743, 361–371. doi:10.1016/j.msea.2018.11.073

Zhang, Y., Zuo, T. T., Tang, Z., Gao, M. C., Dahmen, K. A., Liaw, P. K., et al. (2014). Microstructures and Properties of High-Entropy Alloys. *Prog. Mater. Sci.* 61, 1–93. doi:10.1016/j.pmatsci.2013.10.001

Zhao, J., and Jiang, Z. (2018). Thermomechanical Processing of Advanced High Strength Steels. *Prog. Mater. Sci.* 94, 174–242. doi:10.1016/j.pmatsci.2018.01.006

Zhao, Y. H., Liao, X. Z., Jin, Z., Valiev, R. Z., and Zhu, Y. T. (2004). Microstructures and Mechanical Properties of Ultrafine Grained 7075 Al alloy Processed by ECAP and Their Evolutions during Annealing. *Acta Materialia* 52, 4589–4599. doi:10.1016/j.actamat.2004.06.017

Zhao, Y. L., Yang, T., Tong, Y., Wang, J., Luan, J. H., Jiao, Z. B., et al. (2017). Heterogeneous Precipitation Behavior and Stacking-Fault-Mediated Deformation in a CoCrNi-Based Medium-Entropy alloy. *Acta Materialia* 138, 72–82. doi:10.1016/j.actamat.2017.07.029

Zhao, Y., Topping, T., Bingert, J. F., Thornton, J. J., Dangelewicz, A. M., Li, Y., et al. (2008). High Tensile Ductility and Strength in Bulk Nanostructured Nickel. *Adv. Mater.* 20, 3028–3033. doi:10.1002/adma.200800214

Zhu, T., and Li, J. (2010). Ultra-strength Materials. *Prog. Mater. Sci.* 55, 710–757. doi:10.1016/j.pmatsci.2010.04.001

Zhu, Y., Ameyama, K., Anderson, P. M., Beyerlein, I. J., Gao, H., Kim, H. S., et al. (2020). Heterostructured Materials: superior Properties from Hetero-Zone Interaction. *Mater. Res. Lett.* 9, 1–31. doi:10.1080/21663831.2020.1796836

Zhu, Y. T., Liao, X. Z., and Wu, X. L. (2012). Deformation Twinning in Nanocrystalline Materials. *Prog. Mater. Sci.* 57, 1–62. doi:10.1016/j.pmatsci.2011.05.001

Zhu, Y., and Wu, X. (2019). Perspective on Hetero-Deformation Induced (HDI) Hardening and Back Stress. *Mater. Res. Lett.* 7, 393–398. doi:10.1080/21663831.2019.1616331

Zhu, Z. G., Nguyen, Q. B., Ng, F. L., An, X. H., Liao, X. Z., Liaw, P. K., et al. (2018). Hierarchical Microstructure and Strengthening Mechanisms of a CoCrFeNiMn High Entropy alloy Additively Manufactured by Selective Laser Melting. *Scripta Materialia* 154, 20–24. doi:10.1016/j.scriptamat.2018.05.015

Conflict of Interest: The authors declare that the research was conducted in the absence of any commercial or financial relationships that could be construed as a potential conflict of interest.